Hydrological Processes

WILEY

RESEARCH ARTICLE OPEN ACCESS

Multiscale Analysis of Sediment Dynamics Associated With Reservoir Flushing Operations

Tulio Soto Parra[1] | Giulia Stradiotti[2] | Sebastiano Piccolroaz[1] | Giuseppe Roberto Pisaturo[3] | David Farò[4] | Maurizio Righetti[2,5] | Luigi Fraccarollo[1] | Guido Zolezzi[1]

[1]Department of Civil, Environmental, and Mechanical Engineering, University of Trento, Trento, Italy | [2]Competence Centre for Mountain Innovation Ecosystems, Free University of Bozen-Bolzano, Bozen-Bolzano, Italy | [3]Faculty of Engineering, Free University of Bozen-Bolzano, Bozen-Bolzano, Italy | [4]Leibniz Institute of Freshwater Ecology and Inland Fisheries, IGB Berlin, Berlin, Germany | [5]Faculty of Agricultural, Environmental and Food Sciences, Free University of Bozen-Bolzano, Bozen-Bolzano, Italy

Correspondence: Tulio Soto Parra (tulio.soto@unitn.it)

Received: 9 October 2024 | **Revised:** 23 March 2025 | **Accepted:** 27 April 2025

Funding: This work was supported by Ministero dell'Università e della Ricerca. HORIZON EUROPE Marie Sklodowska-Curie Actions. Interreg Alpine Space program.

Keywords: alpine river | dams | reservoir flushing | reservoir management | sediment management | suspended sediment dynamics

ABSTRACT

The ecological effects of sediment flushings from artificial reservoirs have been widely documented, but the underlying sediment dynamics are less well known. We investigated sediment dynamics associated with a long flushing event divided into two periods (2 and 1 week) in an Alpine river, each followed by a clear water release ('washing') from the reservoir. Suspended sediment dynamics were investigated at the event and annual time scale, and at the river segment (~1000 channel widths) and reach (~100 channel widths or less) spatial scales. Analysis of suspended sediment concentration (SSC) and streamflow time series from 5 in situ calibrated optical turbidity sensors reveals a downstream decrease in the total passing sediment fluxes, a spatial trend that is paralleled by the theoretical suspended sediment transport capacity, allowing for the estimation of the deposited fine sediment volume in different reaches. Washing events result in variable effects among reaches, with some experiencing net sediment entrainment and others net deposition. Out of 16 quantified sediment fluxes, 5 were statistically significant with $p < 0.05$, with an average uncertainty of 23% in fine sediment flux quantification. Georeferenced analysis of coloured gravel-cobble plots before and after the two flushing events revealed partial reach-scale mobility of the coarse bed surface material, particularly in the geomorphic units located at lower elevations and more exposed to higher flows (edges of side bars nearby riffles or rapids), while local fine sediment deposition was observed at less exposed units, such as side channels or point bars in river bends. Grain size distributions of surface sediment taken in the same locations before and 1 month after the flushing reveal a clear shift towards a finer sediment composition, which is partially retrieved also 1 year after the event. Event-averaged SSC values during the flushing are considerably higher compared to natural flood events in such a regulated river, with SSC-streamflow relations being highly irregular and event-dependent, especially during the flushing. The work shows the relevance of multi-scale (time and space) investigation of sediment dynamics for planning and monitoring sediment flushing from artificial reservoirs.

1 | Introduction

Dams and reservoirs disrupt the longitudinal continuity of rivers, thereby interrupting the natural cycle of sediment (Carolli et al. 2023; Belletti et al. 2020). This disruption has significant implications for downstream river morphology, bed composition, ecosystem health and overall biological productivity (Kondolf 1997; Petts and Gurnell 2005; Wohl et al. 2015). In addition, the gradual accumulation of sediment behind dams leads to a reduction in reservoir storage capacity, resulting in potential economic challenges (White 2001) and threatening the safety and operation of reservoirs by obstructing intakes and damaging tunnels or turbines (Morris and Fan 1998; Schleiss et al. 2016).

The theoretical global storage capacity of reservoirs is approximately 7000 km^3, with nearly half of this capacity, around 3000 km^3, lost due to sedimentation (ICOLD 2009). Sedimentation causes an annual loss of approximately 1% of the total storage capacity worldwide (Mccartney et al. 2001; Vörösmarty et al. 2003), resulting in an estimated cost of approximately $21 billion (ICOLD 2009). Looking at the future, the ICOLD (2009) bulletin projects a further global loss of storage capacity amounting to nearly 64% by 2050.

Significant advancements have been made in strategies to address sediment accumulation behind dams in recent decades (Wang and Chunhong 2009; Kondolf et al. 2014). These strategies can be categorised based on the phase in which they are implemented, leading to three distinct approaches: (1) bypassing the incoming fluxes of sediment downstream of dams, accomplished through the construction of bypass tunnels (Sumi et al. 2004; Auel and Boes 2011); (2) removing sediment that has already accumulated in reservoirs, which involves approaches such as reservoir flushing, dredging and excavation (Wang and Chunhong 2009) and (3) minimising the influx into reservoirs, using, for example, off-channel reservoir storage (Kondolf and Farahani 2018). The first and third approaches aim to prevent sediment deposition within the reservoir, while the second strategy directly tackles the challenge of managing sediment accumulation behind dams. Among the existing reservoirs, the predominant strategies fall into the second category, which offers the advantage of not requiring major modifications to the reservoir's structure (Kondolf et al. 2014), and are the focus of the present work.

Hydraulic methods, such as drawdown and pressure flushing, are considered the most cost-effective alternatives for addressing reservoir siltation (Brandt 2000; Kondolf et al. 2014). During drawdown flushing, sediment removal is accomplished by opening the bottom outlets of the dam and lowering the water levels in the reservoir. This process generates flows with velocities capable of eroding and flushing away the accumulated sediment. Pressure flushing is a variation of drawdown flushing that specifically targets the removal of sediment accumulated near the dam. In this method, the dam outlets are opened, but the reservoir's water level is not lowered significantly, and erosion occurs only within a small cone-shaped region upstream of the bottom outlets. Implementing these strategies incurs costs associated with the loss of stored water, temporary interruptions in hydropower production and potential impacts on other productive uses of the dam. Drawdown flushing has been widely adopted in the Alpine region (e.g., Crosa et al. 2010; Grimardias et al. 2017; Legout et al. 2018; Espa et al. 2019; Antoine et al. 2020; Folegot et al. 2021) as it has been found especially effective in elongated and narrow reservoirs. Reservoir flushing, however, can have significant impacts on the morphological and ecological conditions of rivers downstream of dams (Rathburn and Wohl 2001; Crosa et al. 2010; Bilotta et al. 2012). The sudden release of large volumes of sediment into the river downstream of a dam can alter water chemistry, impair water quality and clog the river bottom (Wharton et al. 2017), thereby negatively affecting macroinvertebrate populations (Peter et al. 2014; Folegot et al. 2021), fish communities (Crosa et al. 2010; Kjelland et al. 2015; Baoligao et al. 2016) and the overall aquatic ecosystem.

Despite the ongoing improvements and adaptations made to sediment flushing operations in recent years, aimed at mitigating the adverse environmental effects observed in early monitored experiences (e.g., Wohl and Cenderelli 2000; Espa et al. 2016), a comprehensive understanding of the related sediment transport dynamics occurring in the downstream river channel still presents several gaps.

Most studies on reservoir flushing operations focus primarily on observing ecological aspects in the downstream river reach, to quantify the effects of reservoir flushing on benthic invertebrates (Espa et al. 2013, 2016; Peter et al. 2014; Folegot et al. 2021), fish communities (Crosa et al. 2010; Grimardias et al. 2017; Pisaturo et al. 2021) and water quality (Chung et al. 2008; Lepage et al. 2020; Palanques et al. 2020). Several studies have emphasised the morphological variations and the changes in sediment composition of the riverbed resulting from the flushing waves in the river channel. These studies address the dynamics of both coarse sediment (Wohl and Cenderelli 2000; Brandt 2000; Petts and Gurnell 2005) and suspended sediment associated with reservoir flushing events (e.g., Brandt and Swenning 1999; van Maren et al. 2011; Antoine et al. 2020). However, studies on sediment dynamics related to reservoir flushing events often lack a multi-scale (spatial and temporal) approach and rarely provide a comparison between flushing and natural sediment-transporting floods in the same river sections. In addition, most studies also neglect the uncertainties associated with sediment budget estimations, which were found to reach values of up to 25%, as reported in a similar study in the Arc River, France (Antoine et al. 2020).

Standard monitoring practices for suspended sediment concentration (SSC) during flushing events commonly involve the use of off-the-shelf optical turbidity sensors, which are employed to estimate SSCs (Davies-Colley and Smith 2001). These sensors typically measure light scattering at various angles (e.g., Nephelometric Turbidity Units, NTU), and their accuracy depends on a calibration procedure that correlates turbidity values with sediment concentration (Minella et al. 2008). However, flushing events that reach flood magnitudes can trigger incipient bedload transport, requiring additional techniques to monitor sediment transport more comprehensively (Surian et al. 2009). One traditional field method for monitoring bedload transport involves the use of painted pebbles or trackers, which can be

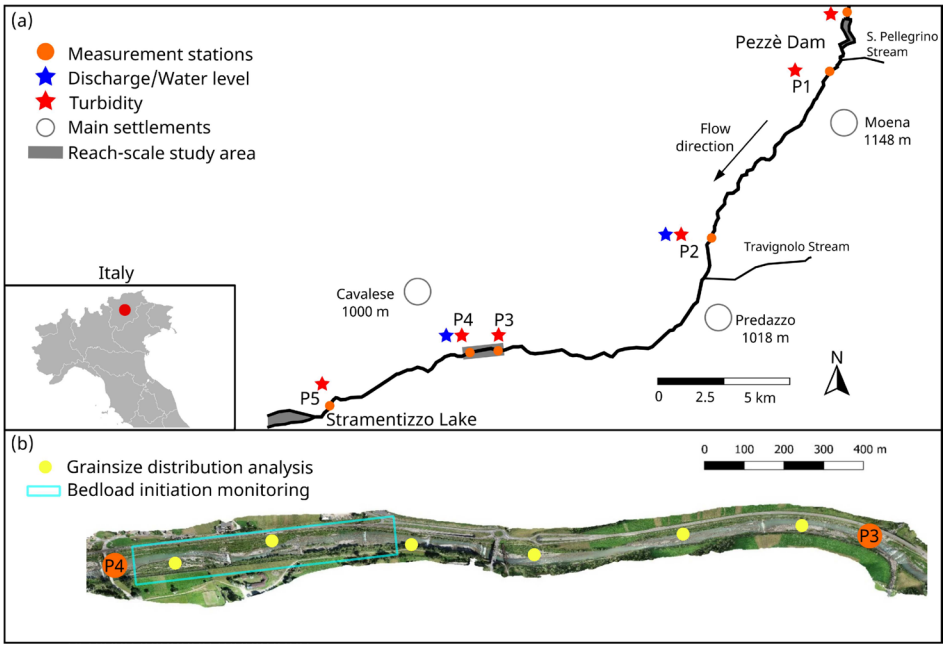

FIGURE 1 | (a) Avisio River segment downstream of the Pezzè dam, showing the locations of discharge/water level and turbidity measurement stations. (b) Reach-scale study area, indicating surface sediment sampling sites and the areas covered by painted gravel plots for bedload initiation monitoring. The aerial photo in panel (b) was provided by Servizio Bacini montani and Nucleo Elicotteri—Vigili del Fuoco of the Autonomous Province of Trento.

tracked after the event to provide quantitative or qualitative estimates, depending on the specific objectives of the study. In some cases, painted square plots are also employed to estimate the extent and movement of bedload (Mao and Surian (2010)).

In this research, we aim to contribute to understanding suspended sediment dynamics associated with dam flushing operations. We investigated the drawdown flushing of a reservoir in the central-eastern Italian Alps (Trentino-South Tyrol), in May–June 2019 as a case study, considering multiple time and space scales. The study was designed to achieve three main research objectives. Our first objective was to quantify the mass of suspended sediment transported downstream of the flushed reservoir, explicitly accounting for uncertainties in its estimation associated with discharge and SSC measurements. Secondly, we aimed at detecting changes in bed surface sediment composition before, shortly after, and 1 year post-flushing. The third objective was to compare the relations between flow rate and suspended sediment load time series associated with the reservoir flushing and with natural flood events at one station. Overall, this study contributes to our understanding of sediment dynamics resulting from reservoir flushing in downstream reaches, offering valuable insights for better management of these operations and mitigation of potential downstream impacts.

2 | Study Area

2.1 | Catchment and General Hydromorphological Characteristics

The Avisio River is a mountain stream that flows through the central-eastern Italian Alps (Figure 1b). Stretching approximately 91 km in length, it features a mean slope of around 21% and drains a basin area of 940 km^2, comprising two distinct geomorphological regions. The first region extends from its source at an elevation of 3331 ma.s.l. in the Marmolada Glacier to just upstream of the village of Predazzo, at an altitude of approximately 1100 ma.s.l., and is characterised by a narrow and steep valley. The second region, from Predazzo to the confluence with the Adige River at 195 ma.s.l, partly encompasses a wider valley with mild slopes (< 1%). The flow regime in the Avisio basin is typically alpine, with intense precipitation occurring during the summer and autumn seasons (mean annual precipitation of 993 mm in the catchment, Provincia Autonoma di Trento 2006), and high flows during spring induced by snowmelt. The Avisio basin contains a total of 51 lakes covering an area of 2.57 km^2, including four artificial reservoirs constructed for hydropower generation. Besides the Pezzè reservoir, the Avisio River is also dammed upstream in the Fedaia reservoir and downstream in the Stramentizzo reservoir, while one of its main tributaries, the Travignolo, is impounded by the Forte Buso dam in the Paneveggio area (Provincia Autonoma di Trento 2006).

The study area encompasses a ~26 km long segment that extends from the Pezzè reservoir to the Stramentizzo reservoir (see Figure 1a). In this segment, the Avisio River primarily features a single-thread channel with a sinuous, channelized pattern and an average slope of 1.5%. The active channel width expands from about 10 m in the upstream, steeper section just downstream of the Pezzè dam to nearly 90 m in the sinuous - wandering, gently sloping sections near Cavalese (Figure 1c), and then narrows to about 30 m in the confined sinuous reaches just before entering the Stramentizzo lake. The river is confined by artificial embankments or bank protection structures. In the few reaches where the channel widens, it forms bars and locally tends to a wandering channel pattern with some stable vegetated island. In the entire section, the channel

TABLE 1 | Summary of instrumentation, data collection techniques and data analysis methods applied in this study.

Station	Instruments	Data collection techniques	Data analysis methods
P1	Turbidimeter	Water sampling for calibration (turbidimeter)	Discharge reconstruction Suspended sediment flux computation Local mass balance computation + uncertainty analysis
P2	Turbidimeter Water level gauge	Water sampling for calibration (turbidimeter)	Discharge measurement Suspended sediment flux computation Local mass balance computation + uncertainty analysis
P3	Turbidimeter	Water sampling for calibration (turbidimeter)	Discharge reconstruction Suspended sediment flux computation Local mass balance computation + uncertainty analysis
P3-P4		Surface sediment sampling (pre, 1 month, 1 year later) Bed surface painting	Grain size distribution analysis Bedload initiation evaluation
P4	Turbidimeter Water level gauge	Water sampling for calibration (turbidimeter)	Discharge measurement Suspended sediment flux computation Local mass balance computation + uncertainty analysis Hysteresis analysis
P5	Turbidimeter	Water sampling for calibration (turbidimeter)	Discharge reconstruction Suspended sediment flux computation Local mass balance computation + uncertainty analysis

slope is regulated by nearly 40 grade control structures. In its wider sections, the Avisio River maintains an average slope of approximately 1.0% with low-height weirs spaced several 100 m apart.

Downstream of the Pezzè di Moena reservoir, the reach is under residual-flow conditions and regulated to a minimum environmental flow, for which the daily-averaged discharge is equal to 1.89 m^3/s. The water collected in the Pezzè di Moena reservoir is sent to the hydropower plant located in Predazzo (Figure 1) through a penstock, and later released back into the Avisio, inducing hydropeaking at the hourly scale; in this segment the daily-averaged discharge is equal to 7.87 m^3/s. During spring, water discharge in the Avisio basin is significantly influenced by snowmelt, making this period crucial for flushing operations.

2.2 | Pezzè Reservoir Characteristics

The Pezzè reservoir, located near the village of Soraga, serves as an artificial reservoir for hydropower production on the Avisio River (Figure 1a). It contributes to the energy production of the Predazzo hydropower plant, with a nominal power of 15 MW, which is situated ~11 km downstream. The reservoir has a nominal capacity of ~460,000 m^3, and an active capacity of ~360,000 m^3. The previous three flushings occurred in 2009, 2012 and 2016, releasing an estimated 55,000 m^3, 21,000 m^3 and 30,000 m^3 of sediment, respectively, as reported by the hydropower company.

Flushing of the Pezzè reservoir typically occurs every 3–4 years during the spring season, when the increasing temperatures promote sufficient snowmelt to allow flushing operations without heavily compromising subsequent hydropower production. Additionally, the Forte Buso dam, located on the Travignolo lateral tributary, also conducts periodic flushing operations, with the most recent occurring in June 2020.

In October 2018, Storm Vaia, an extreme weather event affecting the northeastern Italian Alps, brought exceptionally strong winds coupled with heavy precipitation locally exceeding a 200-year return period. The storm triggered extensive landslides, altered basin morphology, and uprooted approximately 8.5 million cubic metres of trees, many of which were transported into reservoirs (Boretto et al. 2021; Rainato et al. 2021). Given the significant geomorphological disturbances caused by Vaia, it is reasonable to expect that sediment availability in the system has increased, potentially leading to higher sediment volumes being released during subsequent flushing operations, particularly the one addressed in this study.

3 | Material and Methods

Monitoring occurred via continuous and discrete measurements. Some of the instrumentation was specifically installed for the flushing monitoring, while some is permanently monitoring the area, managed by public authorities. Table 1 summarises the data collection and analysis methods used in

relation to each station, while the following sections provide detailed descriptions.

3.1 | Turbidity, Hydrometric Measurements and Computation of Sediment Fluxes

Five turbidity sensors were installed along the studied river segment, in the locations shown in Figure 1a. In this study, we denote the measuring stations by P_i, with i increasing from upstream to downstream. Station P1 was equipped with a fixed monitoring station installed by the local environmental protection agency (APPA Trento), which measured turbidity. Downstream of P1, three optical turbidimeter probes DS5 Hydrolab (with an accuracy within 5% for turbidity values above 400 Nephelometric Turbidity Units or NTU, which is a measurement of light scattered by suspended particles), were installed at stations P2, P3 and P5. Additionally, at station P4, a turbidity sensor model Hach SC 2983400 (accuracy within 5% for turbidity values below 1000 NTU) was installed alongside the 'Masi di Cavalese' hydrometer managed by the regional hydrographic service (Ufficio Dighe of the Autonomous Province of Trento), which had been continuously measuring for several years. All turbidity sensors were programmed to acquire measurements at 15-min intervals. Turbid water samples were collected in 1-liter polyethylene bottles from accessible areas near the sensors at each measurement station and stored at 4°C to preserve sample integrity. To determine the mass of fine sediment in the samples, we followed the procedure outlined in Eaton et al. (2005), which involves filtering the samples through pre-weighed glass fibre filters (0.7 μm), drying them at 105°C for 24 h, and reweighing them to quantify the fine sediment concentration in mg/L. These samples had later been used to convert the SSC series units from NTU to mg/L (see Results, Section 4.1).

Water discharge data for all stations were obtained from two hydrometric gauges managed by the regional hydrographic service and available to the public[1] (Figure 1a). The first gauge was situated in the Travignolo tributary, near its confluence with the Avisio River which is located 2 km downstream of station P2. The second gauge was located next to the turbidity sensor at Station P4. After the Vaia storm, its rating curve was partially resurveyed to check data consistency (Figure S1). A third gauge is found at station P2, where, at the time of the flushing, only water level data were available, and was used as a reference to study the propagation of hydraulic waves.

At each station P_i, the instantaneous mass flux of suspended sediment m_{P_i} is computed by multiplying discharge and SSC:

$$m_{P_i}(t) = Q_{P_i}(t) \cdot C_{P_i}(t), \tag{1}$$

where t denotes time, $Q_{P_i}(t)$ is the discharge, and $C_{P_i}(t)$ is the SSC at station P_i at time t, which is assumed to be homogeneous across the river section. Moreover, by integrating the instantaneous fluxes over a chosen period T, the total mass of suspended sediment load passing at each station P_i over that period is computed as:

$$M_{P_i} = \int_{t_0}^{t_0+T} Q_{P_i}(t) \cdot C_{P_i}(t)\,dt, \tag{2}$$

where t_0 indicates the starting time of the period.

Finally, calculating the local sediment mass balance between consecutive stations P_i and P_{i+1} provides insights into the occurrence of potential net suspended sediment deposition or net erosion during the flushing event, assuming that SSC exchanges in the lateral direction (e.g., bank erosion or floodplain sedimentation) and the input from lateral tributaries is negligible. Therefore:

$$\Delta M_{P_i - P_{i+1}} = M_{P_i} - M_{P_{i+1}}, \tag{3}$$

with positive values of Δ suggesting deposition in the subreach between P_i and P_{i+1}, and negative values suggesting erosion.

3.2 | Uncertainty in the Estimation of Sediment Fluxes

The computation of instantaneous suspended sediment fluxes is based on measurements and calculations of discharge and SSC. To account for the uncertainties associated with these procedures, an uncertainty propagation model is proposed in the form of the following equation (Antoine et al. 2020):

$$u_m = \sqrt{u_Q^2 + u_C^2}, \tag{4}$$

where u_m is the relative variance of suspended sediment fluxes; u_Q is the standard relative uncertainty of discharge; and u_C is the standard relative uncertainty of SSC. Moreover, it is necessary to break down each relative variance to allow for all significant sources of uncertainty (Ku 1966).

In discharge time-series, three main sources of uncertainty should be considered: (1) the stage-discharge relation or rating curve ($u_{Q_{HQ}}$), (2) the effect of linear interpolation ($u_{Q_{int}}$) between the measured discharge values and (3) the unaccounted water contributions from smaller lateral catchments ($u_{Q_{ukn}}$). Moreover, in this study, we identified an additional source of uncertainty denoted as Q_{lag}, arising from the shifting of discharge hydrographs to upstream and downstream stations. This term explicitly accounts for potential misalignments in discharge hydrographs, which can significantly impact the accuracy of total sediment load estimates. As a result, u_Q can be expressed as:

$$u_Q = \sqrt{u_{Q_{HQ}}^2 + u_{Q_{int}}^2 + u_{Q_{ukn}}^2 + u_{Q_{lag}}^2} \tag{5}$$

Concerning SSC time-series, we identified five main sources of uncertainty, after Antoine et al. (2020) and Misset et al. (2019): the (1) vertical ($u_{C_{vh}}$) and (2) transverse ($u_{C_{th}}$) spatial heterogeneity of the SSC in a river cross-section; (3) the calibration procedure and derivation of NTU-SSC relationships for the turbidity sensors ($u_{C_{reg}}$); (4) the accuracy of the turbidity sensors ($u_{C_{Tu}}$) and (5) the effect of the sampling frequency $u_{C_{int}}$. The contribution of the five sources leads to the overall SSC-uncertainty u_C:

$$u_C = \sqrt{u_{C_{vh}}^2 + u_{C_{th}}^2 + u_{C_{reg}}^2 + u_{C_{Tu}}^2 + u_{C_{int}}^2} \tag{6}$$

3.3 | Suspended Sediment Transport Capacity

The estimates of suspended sediment transport can be complemented by the estimate of the reach-average suspended sediment (SS) transport capacity, and the corresponding total volumetric reach transport capacities on a specified period. To this aim, we adopted the approach proposed by Chanson 2004, based on the well-known empirical formula by Van Rijn (1984a). The total SS volume corresponding to the estimated transport capacity for each homogeneous subreach over a time period T can be approximated using the following equation:

$$V_{P_i-P_{i+1}} = \int_{t_0}^{t_0+T} \overline{\phi}(t) \cdot Q_{P_i}(t)\, dt, \tag{7}$$

where $V_{P_i-P_{i+1}}$ is the total volumetric SS transport capacity of subreach $P_i - P_{i+1}$; $\overline{\phi}$ is Rouse's depth-averaged modeled SSC for $P_i - P_{i+1}$ (see section S1 for details on how it was computed) and Q_{P_i} is the streamflow series at the P_i station. To determine the average channel width and slope for each subreach needed for the calculations, we analysed high-resolution orthophotos and digital terrain models (DTM, at 0.5 m resolution) of the region, made available to the public by the WebGIS service of the Province of Trento[2].

3.4 | Grain Size Distribution Analyses

The effect of the flushing at the reach scale was further assessed by monitoring the changes in the surface sediment grain size distribution in reach P3–P4. Surface sediment samples were collected at five designated sampling locations along the 2 km reach located between P3 and P4, about 20 km downstream of the dam (Figure 1c). The samples were obtained using a flat-blade shovel, which was inserted approximately 15 cm into the riverbed surface sediment and carefully scooped out into plastic buckets. The samples were oven-dried at 105°C for 24 h and mechanically sieved to determine the grain size distribution before the flushing event (as reference conditions, referred to as 'PRE'), 1 month after the flushing (referred to as 'POST1') and 1 year after the flushing (referred to as 'POST2'). By comparing grain size distributions between PRE and POST1, we could quantify the textural alteration induced by the flushing event, and by comparing POST1 and POST2 it was possible to assess the effects of the flow regime in the year that followed the flushing. The analysis was conducted using standard laboratory procedures, which involved drying and sieving the collected samples. The particle size scale proposed by Blott and Pye (2012) was employed for the grain size characterisation.

3.5 | Bedload Initiation Monitoring

Bedload transport initiation was monitored using coloured tracers following a well-established practice in river morphology studies (e.g., Church and Hassan 1992). To achieve this, a simple and inexpensive method was employed, which involved painting the surface layer of the river bed with fast-drying paint (Mao and Surian 2010). The selected locations for painting were expected to be later submerged during the flushing. Following the procedure described by Mao and Surian (2010), squared surfaces measuring 1 × 1 m were painted at 10 different locations along the 2 km reach between P3 and P4. The painting was carried out 3 days before the start of the flushing, and the control survey was conducted 1 month after. The selection of locations took into consideration the presence of various morphological units (Belletti et al. 2017) and aimed to be as close as possible to the edges of banks, islands and emerging bars that were dry at low flow conditions before the flushing and were likely to be inundated during the flushing. To assess bedload transport dynamics, this analysis focuse on the morphological unit where the plot was located, the presence of vegetation cover, the location of the plot on the bar/unit, and the observed effects.

3.6 | Suspended Sediment Dynamics in Reservoir Flushing Versus Natural Floods

The discharge and turbidity measuring station installed in P4 recorded data on both natural flood events and the flushing operation in the Avisio River. Thus, to ensure consistency and avoid introducing uncertainties related to assumptions about hydraulic and turbidity wave dynamics, data collected only at station P4 were used for comparing flushing and natural events in terms of SSC dynamics. A hysteresis analysis was used to describe the non-linear relationships between the discharge and turbidity. Hysteresis loops occur during storm events due to the time lag between discharge and turbidity signals, which causes the turbidity at a given discharge on the rising limb of the hydrograph to differ from that on the descending limb. The shape and size of the hysteresis loop depend on sediment transport dynamics, with clockwise hysteresis indicating proximal and rapidly mobilised sediment sources and indicating that the peak concentration occurs ahead of the peak discharge, while counterclockwise hysteresis reflects either near-stream channel sources with slow travel times or distal sources (Zuecco et al. 2016). Storm events can exhibit complex hysteresis patterns due to spatial and temporal variability in precipitation and runoff, making comparisons challenging (Williams 1989).

For all the recorded events, natural and artificial, a hysteresis index (HI) after Zuecco et al. (2016), and a normalised slope index (NS) after Vaughan et al. (2017); Wymore et al. (2019) were calculated. HI values range from −1 to 1, with negative values describing a counterclockwise hysteresis, positive values indicating a clockwise hysteresis, and $HI = 0$ indicating no hysteresis or a symmetrical eight-shaped or complex loop (Zuecco et al. 2016). To compute HI discharge and SSC data has to be normalised, as follows:

$$\widehat{Q}(t) = \frac{Q(t) - Q_{min}}{Q_{max} - Q_{min}}\ ,\ \widehat{C}(t) = \frac{C(t) - C_{min}}{C_{max} - C_{min}}\ , \tag{8}$$

where $Q(t)$ and $C(t)$ are the two variables at time t; Q_{min} , Q_{max} , C_{min} , C_{max} are the minimum and maximum values of discharge (Q) and SSC (C), and $\widehat{Q}(t)$, $\widehat{C}(t)$ are the normalised values of $Q(t)$ and $C(t)$, respectively. Then, the differences between definite integrals and the rising and falling limbs can be computed as:

$$\Delta A_{[i,j]} = A_{r[i,j]} - A_{f[i,j]} = \int_i^j C_r\left(\hat{Q}\right) d\hat{Q} - \int_i^j C_f\left(\hat{Q}\right) d\hat{Q} \quad (9)$$

where $\Delta A_{[i,j]}$ is the difference between the definite integrals $A_{r[i,j]}$ on the rising and $A_{f[i,j]}$ on the falling limbs for a given interval i, j ranging from $\hat{Q} = 0$ to $\hat{Q} = 1$. Finally, *HI* is computed as the sum of these definite integrals:

$$HI = \sum_{k=1}^{n} \Delta A_{[i,j,k]} \quad (10)$$

where n is the number of intervals, and k is the summation index that iterates through each interval. In this work, we selected an interval of 0.05 covering the range from $\hat{Q} = 0.15$ to $\hat{Q} = 1$.

Normalised slope index (NS), also known as Flushing Index (FI), described by Wymore et al. 2019, characterises the slope of the line that links the normalised concentration values at the beginning and peak of the normalised discharge. NS ranges from −1 to 1, with negative values suggesting dilution on the rising limb related to source-limited material export, and positive values indicating flushing on the rising limb, associated with increased concentration and transport-limited delivery of material (Vaughan et al. 2017). *NS* can be computed as $NS = \hat{C}_{Q_{peak}} - \hat{C}_{Q_{init}}$, with $\hat{C}_{Q_{peak}}$ the concentration at peak flow, normalised to the maximum concentration value measured during the storm; and $\hat{C}_{Q_{init}}$ the concentration at the beginning of the storm, normalised to the maximum concentration value measured during the event. When the SSC is independent of the discharge, the behaviour is considered chemostatic and does not vary significantly with changes in discharge or water flow. (Godsey et al. 2008). Furthermore, the hysteresis class (Zuecco et al. 2016) describes scenarios where the SSC either primarily increases or decreases during the rising phase of discharge. Finally, the Pearson coefficient was also computed to assess the strength and direction of the linear relationship between SSC and discharge during the events.

Suspended sediment dynamics were compared between three reservoir flushing events and three natural storm-induced flood events. For the flushing events, the two stages of flushing in the Pezzè reservoir were considered: (1) from the start of the flushing on May 15 to the interruption of flushing for the Giro d'Italia event on May 31, and (2) from the resumption of the flushing on June 2 to the closure of the bottom outlets on June 6, 2019. The third flushing event (3) took place between June 11 and 13, 2020, released from the Forte Buso reservoir, located on the Travignolo tributary, which was registered downstream by station P4.

To conduct the hysteresis analysis, a temporal delimitation of the events was required. For the flushing events, the periods mentioned above were used to determine the start and end of each event based on the operation schedules of the dams. However, for natural floods, the definition of the start and end of the events could not be directly inferred from the discharge time series. Therefore, the following approach was adopted to define the flood event duration: (1) the mode discharge value (Q_{Mo}), defined as the most frequently occurring discharge value within the recorded period, was calculated for each natural flood event, including a time buffer of ± twice the visually estimated duration of the event; (2) the last occurrence of Q_{Mo} before the peak flood discharge was selected as the starting point of the event and (3) the first incidence of Q_{Mo} after the peak flood discharge was set as the end of the event. An example of this approach is presented in the Figure S2.

4 | Results

Table 2 includes all physical and hydraulic parameters of the subreaches that are used for all the computations.

4.1 | Discharge and SSC

The discharge series Q_{P_i} (Figure 2a) at each station were computed as follows: Q_{P_4} was directly obtained from the hydrometer gauge; Q_{P_1} and Q_{P_2} were derived by subtracting the discharge of the Travignolo tributary from Q_{P_4}, while considering the time lag intervals associated with the downstream propagation of hydraulic waves; Q_{P_3} and Q_{P_5} were obtained by simply shifting Q_{P_4} to account for the corresponding time lags. To estimate the time lags associated with the hydraulic wave propagation, a cross-correlation analysis was performed between the water level time series from P2 and P4 (Figure 2b). The highest correlation between the two signals was found at a time interval of −105 min, yielding, for a distance of approximately 12.5 km, an event-average wave celerity of 1.98 m/s. Discharge data from smaller creeks and small lateral streams were not available and therefore were not quantified; however, their contribution can be considered negligible with respect to the high flow rates occurring during flushing events. As observed in P4, the progressive increase in discharge over time during the flushing event is evident in Figure 2a, with two discharge peaks observed on May 29 and June 8, 2019, reaching a maximum of 64.96 m^3/s. The average discharge over the

TABLE 2 | Physical and hydraulic characteristics of the study site subreaches. The reported D90 corresponds to the bed surface layer, while the fine sediment fraction corresponds to the sample sediment smaller than 2 mm.

Subreach	Length [km]	Mean width [m]	Mean slope [%]	d90 of surface sediment [mm]	d50 of fine sediment fraction [mm]
P1–P2	10.7	12	1.85	185	0.5
P2–P3	8.96	28.9	1.45	185	0.5
P3–P4	2.1	33.8	0.80	185	0.5
P4–P5	4.92	27.4	0.89	185	0.5

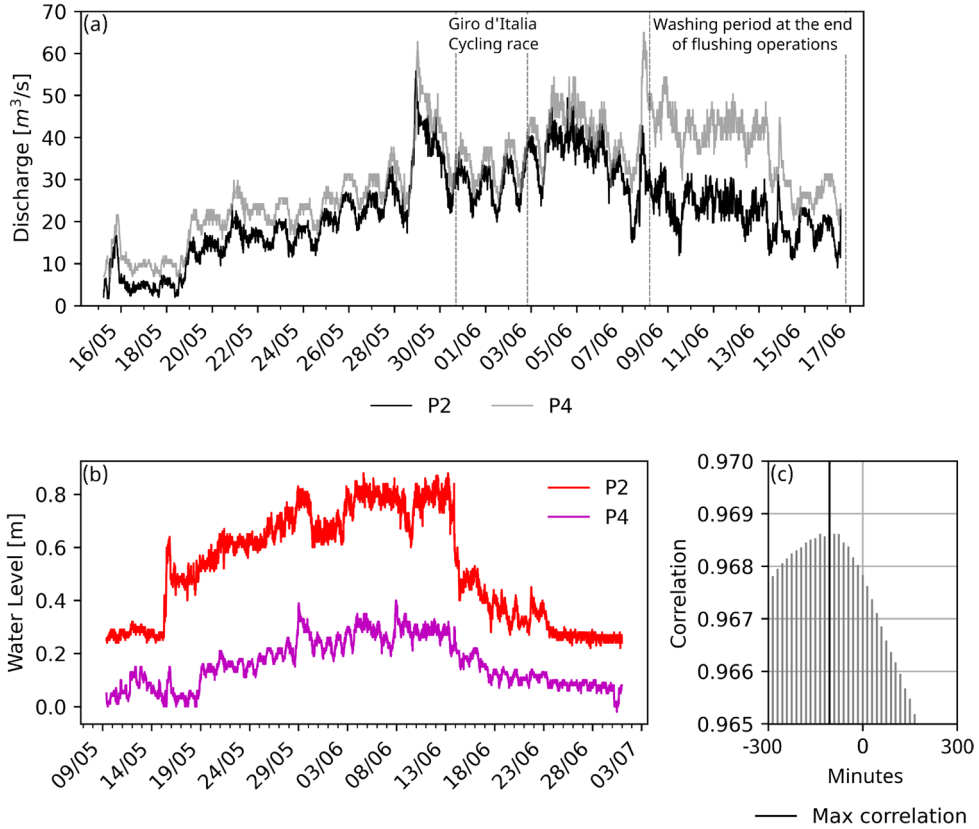

FIGURE 2 | (a) Discharge time series of stations P2 and P4. The discharges at station P1 are similar to those at P2, and the discharges at stations P3 and P5 are similar to those at P4, with a slight temporal shift. A description of the discharge data for all stations can be found in Section 3.1. (b) Water level time series of stations P2 and P4. (c) Cross-correlation analysis of the water level time series signals of stations P2 and P4.

entire flushing period was 29.87 m^3/s, with a median value of 29.81 m^3/s. Flow variability was substantial, as indicated by a standard deviation of 12.27 m^3/s.

The SSC series were measured by the turbidimeters installed in the positions described in Section 3.1, and converted from NTU to mg/L by applying a linear least-squares regression of the form $SSC = a \cdot NTU$ to establish a relationship between the mass of fine sediment (mg/L) collected for the instruments' calibration and the turbidity sensor readings (NTU) recorded at the time of collection. Previous studies (i.e., Merten et al. 2014; Druine et al. 2018; Pallarès et al. 2021) have confirmed the validity of linear relationships between SSC and the output of optical turbidity sensors, such as NTU. In these relationships, the intercept coefficient is often set to 0 since negative values of SSC hold no physical significance. Figure 3 presents the calibration results at each station. The correlation between field measurements (water sample analysis) and optical measurements (continuous sensors) varies across stations, with RMSE values ranging from 400 to 2000 mg/L, and the standard error of the regression coefficients ranging from 10% to 19%, as shown in Figure 3. The resulting SSC time series for each station is shown in Figure 4. The turbidity sensor at station P2 experienced a temporary malfunction, resulting in a data gap from May 27, 01:45 to May 30, 01:00. To fill in the missing data, the mean difference in turbidity values between stations P1 and P2 was calculated for the entire analysis period, adjusted with a 1-h time lag (determined by cross-correlation analysis). This mean difference was then subtracted from the P1 values during the malfunction period to estimate the missing P2 data. The upstream stations, P1 and P2, exhibit SSC values ranging between 100 mg/L and 18,000 mg/L, while in the downstream stations P3, P4 and P5, SSC values in the range 300 mg/L and up to 4800 mg/L (in P3) can be observed. Figure 4 also reveals an abrupt decrease in SSC across all the stations between May 31 and June 3, 2019. This reduction was due to the interruption of the flushing operation during the international cycling race 'Giro d'Italia' as it passed along the Avisio River. The flushing of the Pezzè dam can therefore be viewed as a series of alternated flushing and 'washing' events: (1) an initial flushing (Flushing 1, May 15–30, 2019), (2) a release of clear water pulses or 'river washing period' during the Giro d'Italia (Washing 1, May 30–June 2, 2019), (3) a second flushing event (Flushing 2, June 2–8, 2019), and (4) a second washing period that lasted approximately 6 days starting from June 8, 2019 (Washing 2), during which discharges were kept high to help remove fine sediment deposits accumulated on the riverbed during the flushing operation.

The assumptions, simplifications, and limitations in the assessment of the discharge and SSC time series lead to uncertainties that, in turn, affect the estimate of the suspended sediment fluxes (see Section 3.2). In the following, we analyse the contribution of each source of uncertainty individually.

4.1.1 | Uncertainty of Discharge

The uncertainty of discharge time series is related to four sources (see Equation 5). Among these, the uncertainty for the

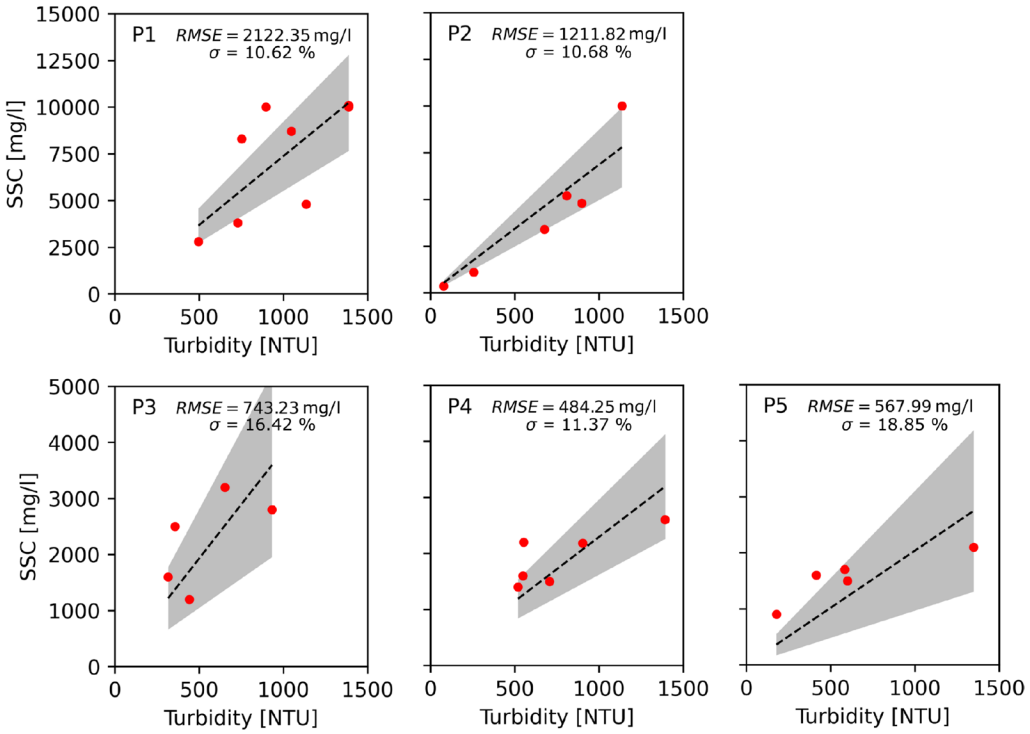

FIGURE 3 | Calibration curve (black dashed line) of turbidity sensors for all stations (the red dots represent the samples used for the calibration), 95% confidence intervals (grey area), RMSE values in mg / L and standard error of regression coefficients (σ).

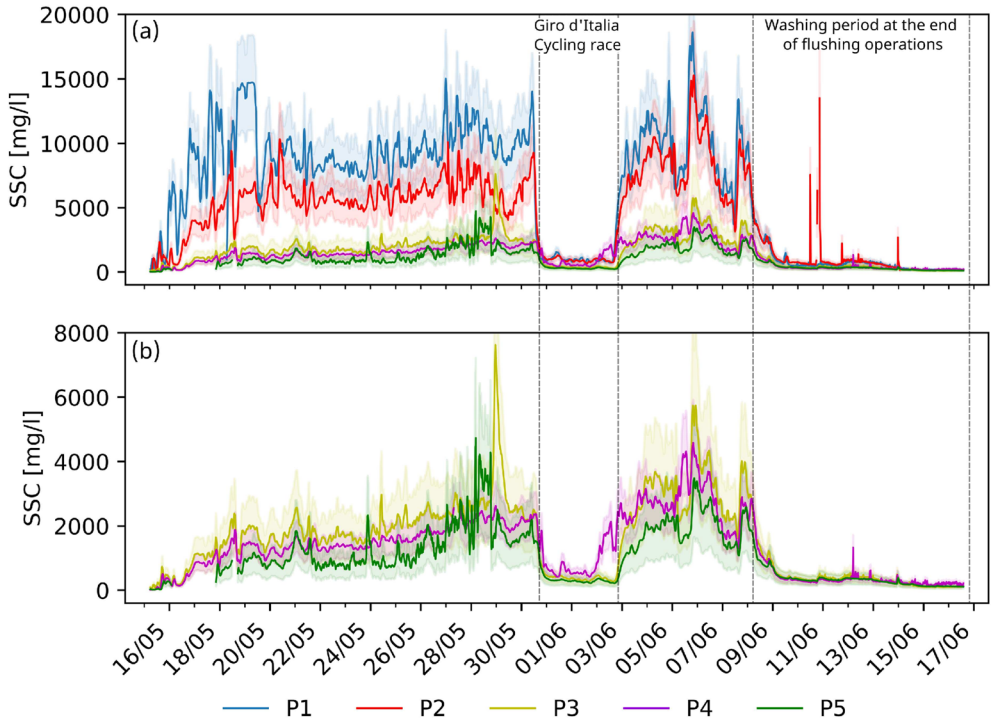

FIGURE 4 | Suspended sediment concentration (SSC, solid lines) time series and confidence intervals (blurred areas): (a) all stations; (b) close-up of stations P3, P4 and P5. Note the different value ranges in the vertical axis. The vertical dashed lines separate river-washing from flushing periods.

unaccounted water contributions ($u_{Q_{ukn}}$) is particularly relevant for stations P1, P2 and P5, where only the addition of the largest stream (Travignolo, Figure 1) was considered. However, we could not account for this source of uncertainty in our calculations, due to missing information. Nonetheless, the flow contributions of unknown magnitudes and sediment concentrations are implicitly accounted for in the measurements from station P4, which is located downstream. Moreover, given the short sampling interval (15 min) in discharge time series, it is possible to neglect the temporal effect of linear interpolation ($u^2_{Q_{int}}$) of

the instantaneous discharge values when computing sediment fluxes, as its effect becomes negligible (Antoine et al. 2020).

Regarding the uncertainty related to potential time series misalignment when shifting the discharge hydrograph ($u^2_{Q_{lag}}$), we determined that for high temporal resolution, extended events, such as the 15-min time interval, month-long dataset analysed here (3106 time steps), localised discrepancies introduced by shifting $Q(t)$ are averaged out across the long integration window, resulting in a negligible overall impact on sediment budgets (see Figure S3). This analysis was included in Section S3 in the Supporting Information.

As a result, the uncertainty of discharge values (u_Q) in this work has been computed based solely on the uncertainty of the rating curve: $u_Q = u_{Q_{HQ}}$.

Site-specific uncertainties of discharge rating curves u_{HQ} have been reported in the literature (e.g., Di Baldassarre and Montanari 2009; Le Coz et al. 2014), with values ranging from 5% up to 42% (Olivier et al. 2008; Di Baldassarre and Montanari 2009). To assess the precision of the discharge rating curve in station P4, three measurements at different discharges were conducted in 2019 at the hydrometer section and can be found in Figure S1. While it demonstrates a very good agreement between the measured and rated discharges ($r^2 = 0.94$), it is important to note that only low-flow discharges were measured. Therefore, the validity of the rating curve for high discharge values, which are likely to be predominant during flushing operations, could not be verified. As a conservative estimate, we assumed an uncertainty of $u_{Q_{HQ}} = 10\,\%$, which is of the same order of magnitude as the uncertainty estimated by Olivier et al. (2008) and chosen by Antoine et al. (2020) in a recent, similar study on the Arc River, which shares hydromorphological characteristics similar to the Avisio.

Finally, the discharge estimate for stations P1, P2 and P3 incorporates data from two hydrometers (Travignolo tributary and P4). Given the lack of available information on the validity of the rating curve at the Travignolo tributary hydrometer, a conservative estimate will assume an additional 10% uncertainty. Therefore, applying the same reasoning, $u_{Q_{P1,P2,P3}}$ is estimated to be 14.14%.

4.1.2 | Uncertainty of Suspended Sediment Concentration

The uncertainty in the suspended sediment time series is dependent on five factors (see Equation 6). The first two sources of uncertainty ($u_{C_{vh}}$ and $u_{C_{th}}$) stem from the assumption of homogeneous SSC values across the entire river cross-section, which may not hold true in the so-called 'near' or 'intermediate' fields downstream of point sediment sources. The spatial distribution of suspended sediment depends on various factors such as the type of SSC sources (point, diffused), distance from the sources, the spatial scales of turbulent diffusion and dispersion processes, grain size distribution and riverbed geometry (Antoine et al. 2020). We evaluated $u_{C_{vh}}$ following Camenen et al. (2018), who proposed a method based on the assumption that the vertical distribution of SSC follows a theoretical Rouse profile. The detailed computation procedure can be found in Section S1 in the Supporting Information. The average value of Rouse number obtained from the calculations in all sections was $P = 0.16$, resulting in a theoretical standard deviation of about 12% for the SSC vertical profile, for which $u_{C_{vh}} = 12\,\%$.

The transverse heterogeneity of SSC depends on the transverse or lateral variability of turbulence, bed roughness (Antoine et al. 2020), the geometry of the channel, and the distance from the sources. Transversal heterogeneity was measured by Némery et al. (2013) in a similar case study of a dam flushing in an alpine river by sampling SSC at the surface along the cross-section, resulting in an average standard deviation of 5% between the middle and sides of the cross-section. In the Avisio case study, the sampling locations were located some tens (P1) to hundreds (P4, P5) channel widths downstream of the main source of fine sediment, therefore suggesting a likely occurrence of transverse mixing of the flushed fine sediment, with transverse heterogeneity being mainly associated with the minor sediment inputs from the smaller lateral tributaries. Following the study of Némery et al. (2013), an indicative value of $u_{C_{th}} = 5\,\%$ has been assumed for our computations.

The uncertainty in the calibration procedure $u_{C_{reg}}$ corresponds to the standard error of the regression coefficients of the NTU-SSC relationships of individual stations derived from laboratory procedures, as explained in Section 3.1 and further outlined in Section 4.1. $u_{C_{Tu}}$ is taken after the reported accuracy of the turbidity sensors (5% for NTU > 400, and 5% for values up to 1000 NTU, for the DS5 HydroLab and Hach respectively). Finally, a conservative value of $u_{C_{int}} = 3\,\%$ was chosen after Antoine et al. (2020), who determined that the uncertainty due to sampling frequency becomes negligible for sampling time intervals of 30 min or lower, with our sampling frequency being 15 min.

4.2 | Suspended Sediment Flux and Local Mass Balance

Table 3 shows the total suspended sediment loads for each station and sub-event computed through equation (2), alongside the overall uncertainty u_m associated with each station (Section 3.2). Figure 5a shows the suspended sediment loads transported during the two flushing sub-events, with the lengths of the error bars indicating the global (for both events) uncertainties associated with the respective stations.

Table 4 summarises the results on the local sediment mass balance, computed following equation (3). By incorporating the uncertainty in the estimation of sediment fluxes it is possible to determine the statistical significance of the local mass balance between two consecutive stations. Therefore, the condition for statistically significant erosion or deposition processes in the river reach between stations $P_i - P_{i+1}$ can be established when the absolute difference in sediment transport rates between two stations $\Delta M_{P_i - P_{i+1}}$ exceeds 1.96 times (critical value for a 95% confidence interval in a standard normal distribution) the square root of the sum of their associated errors (σ_P) (Antoine et al. 2020). Thus:

$$\left|\Delta M_{P_i - P_{i+1}}\right| > 1.96 \cdot \sqrt{\sigma^2_{P_i} + \sigma^2_{P_{i+1}}} \tag{11}$$

TABLE 3 | Total sediment load and estimated global uncertainties u_m for all stations.

Station	Total sediment load M_{P_i} [Tons]							u_m [%]
	Total Sediment	Flushing 1	Flushing 2	Total Flushing	Washing 1	Washing 2	Total Washing	
P1	405082	223643	157453	381096	8710	15276	23986	22.71
P2	296688	140289	130783	271073	8848	16767	25616	22.73
P3	142640	68021	57496	125517	4086	13036	17122	25.93
P4	122250	49438	52516	101954	8218	12077	20296	20.79
P5	90879	40859	36370	77229	3135	10514	13648	25.66

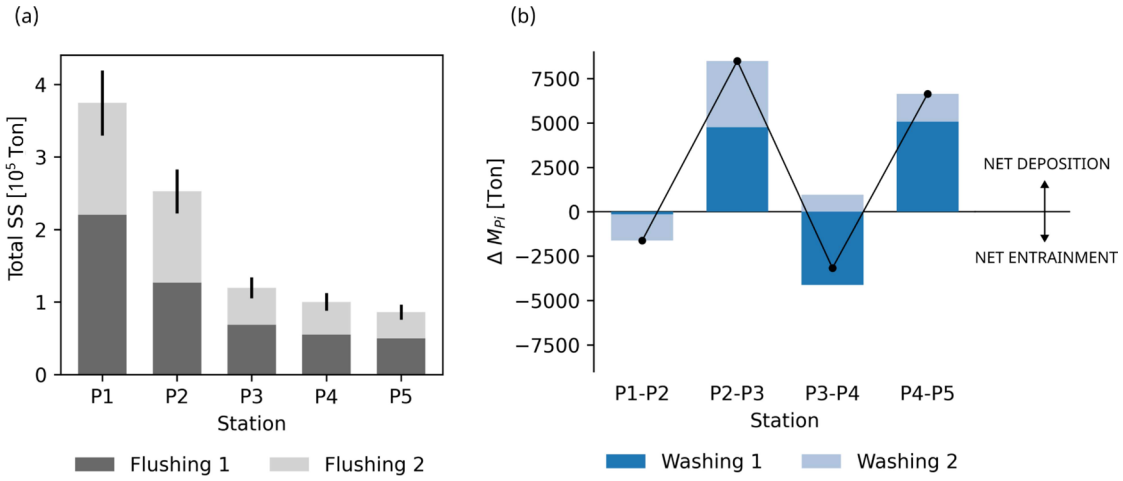

FIGURE 5 | (a) Total mass of passing suspended sediment at each station from both flushing events and estimated errors resulting from the uncertainty analysis described in Section 3.2. (b) Sediment balance during the washing events. Positive values indicate net deposition over the entire washing period while negative values indicate net sediment entrainment.

TABLE 4 | Local sediment mass balance distribution in the flushing of the Pezzè dam, in the Avisio River. Positive values suggest deposition, whereas negative values indicate erosion. Bold values denote statistically significant differences concerning Equation 11.

Subreach	Local sediment mass balance $\Delta M_{P_i-P_i+1}$ [Tons]						
	Total Sediment	Flushing 1	Flushing 2	Total Flushing	Washing 1	Washing 2	Total Washing
P1-P2	108395	83354	26669	110023	−139	−1491	−1630
P2-P3	**154045**	**72268**	**73287**	**145555**	**4762**	3731	8493
P3-P4	20393	18583	4981	23564	**−4132**	959	−3173
P4-P5	31371	8579	16146	24725	**5084**	1563	6647

where $\sigma_{P_i} = M_{P_i} \cdot u_{m_{P_i}}$ and $\sigma_{P_{i+1}} = M_{P_{i+1}} \cdot u_{m_{P_{i+1}}}$. As a result, 5 out of 16 estimated local mass balances (4 subreaches, 2 flushing and 2 washing events) were statistically significant according to the 95% confidence level (indicated in bold in Table 4). This is consistent with the overlapping confidence intervals between SSC times series observed in Figure 4, which indicate that the differences in SSC between consecutive stations are small compared to their uncertainties.

During the flushing events, most local mass balances indicated deposition within the subreaches (positive values in Table 4). Specifically, the statistically significant local mass balance between stations P2 and P3 suggests that an approximate fraction between 32% and 48% of the total flushed sediment loads was deposited in this reach. Figure 5b shows the sediment balance during the washing periods. In the first washing period, between the two flushing sub-events, significant local mass balances

indicate net entrainment in the reach between stations P1–P2 and P3–P4, while net deposition occurred in reaches P2–P3 and the lowermost P4–P5. A similar trend was observed during the second washing period.

4.3 | Suspended Sediment Transport Capacity

We computed the suspended sediment transport capacity through the method outlined in Section 3.3, Equation (7). We divided the river segment into four subreaches between each consecutive pair of stations, and we used the discharge time series of each P_i station to estimate the total SS transport capacity of the subreach $P_i - P_{i+1}$. The water depth, required for estimating suspended sediment transport rates, was computed using the Chézy-Manning uniform flow equation for an equivalent rectangular channel, assuming instantaneous normal flow conditions (Chow 1954). A Manning's roughness coefficient ($0.04\ \mathrm{s \cdot m^{-1/3}}$) suitable for mountain streams was assumed (Chow 1954), and rectangular channel geometry was considered for all subreaches. The characteristic grain size diameters of the surface sediment required for the calculation of SS transport capacity were derived from a previous study on the morphological evolution of the Adige basin by Bergamin (2017). Moreover, the characteristic grain size of the fine sediment was determined as the d_{50} of the fine sediment fraction (< 2 mm) from surface sediment samples collected after the flushing. Table 2 provides a summary of the parameters used in these computations.

Figure 6 reports the comparison between the measured suspended sediment transport and its theoretical capacity, for each station P2–P5. To facilitate the comparison between measured suspended sediment transport (mass) and theoretical transport capacities (volume) across the reaches, we normalised both values relative to their respective totals at station P1. This approach avoids introducing uncertainty from assumed sediment density values and allows for a consistent, relative comparison. The assumption is that the total sediment passing station P1 represents the total flushed sediment from the dam, given its vicinity. In general, the downstream-decreasing trend in normalised measured SS transport (blue bars) is consistent with the analogous trend of the normalised theoretical SS transport capacity from P2 to P5 (red bars, calculation procedure described in Section 3.3), suggesting a downstream decreasing reach transport capacity. Approximately 70% of the total flushed sediment that passed through P1 were transported down to station P2, aligning well with the theoretical estimations. Similarly, stations P4 and P5 exhibit only slight differences between theoretical and observed relative estimates. The measured relative SS mass in P3 indicates that less than 5% of the total transport was retained in the reach between P3 and P4 compared to a relatively higher theoretical transport capacity of 55% of the total transport.

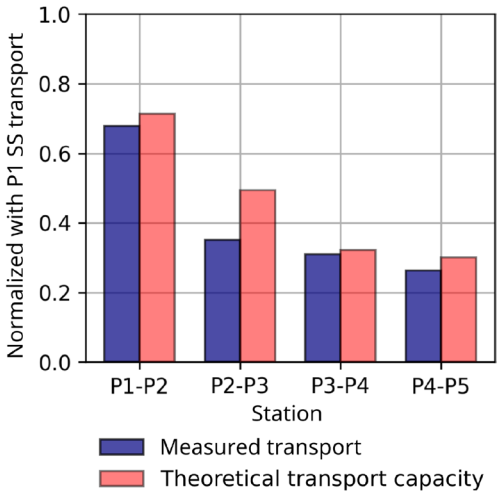

FIGURE 6 | Subreach measured and theoretical suspended sediment transport capacity normalised with respect to the total passing sediment at station P1.

To investigate the sediment dynamics during the washing periods, where the source of SSC is assumed to be exclusively from the riverbed, a closer analysis was conducted (Figure 7a,b). The results indicate that the washing periods were capable of transporting sediment. During the first washing period, the evolution of instantaneous fluxes between stations P3 and P4 results in a gradual reduction of the reach sediment balance. This suggests that dominant sediment entrainment was occurring, leading to a decrease in the deposited sediment (black line). The second washing period, which took place immediately after the end of the reservoir flushing, exhibited a different trend. The progression of sediment balance during this period suggests that deposition processes occurred from June 8 to June 13. However, the negative slope of the mass balance at the end of the period (black line, from June 14) indicates a subsequent resuspension of the sediment.

4.4 | Bed Surface Sediment Composition

The surface sediment sampling survey conducted 1 month after the flushing (POST1) revealed significant deposits of fine sediment distributed throughout the sampling reach, in contrast to the conditions observed prior to the flushing (PRE). These fine sediment deposits formed dunes, accumulated primarily along the shores, areas with low-flow velocities, and backwater channels (as shown in Figure 8). This visual evidence of temporal changes is supported by the analysis of bed surface grain size distributions (Figure S4 in the Supporting Information), also summarised in Figure 9 and Table S1, which details the proportions of gravel, sand, and clay, as well as their net changes after the flushing in all collected samples.

The results from the survey conducted 1 month after the flushing (Figure S4, black dotted lines, and intermediate bars in Figure 9) indicate a shift towards finer grain diameters in all the sampling sites. This shift is evident in the reduction of the percentage of gravel, with a corresponding increase in the proportion of sand (Table S1 in the Supporting Information, POST1). The contribution of clay remains negligible compared to the other grain sizes. One year after the flushing (POST2, darkest right bars in Figure 9), the grain size distribution in sites 2 and 4 showed a partial recovery towards the pre-flushing conditions (Figure S4 black solid line, in the Supporting Information). However, on

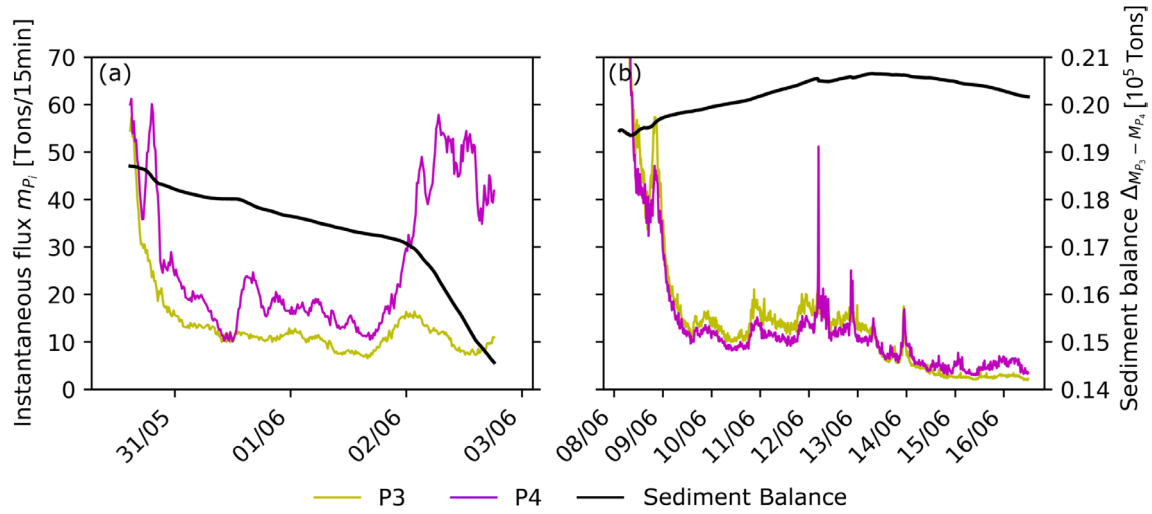

FIGURE 7 | Instantaneous fluxes (yellow line, P3 and magenta line, P4) and cumulative sediment balance (black line) at reach P3–P4. (a) Washing 1 (b) Washing 2.

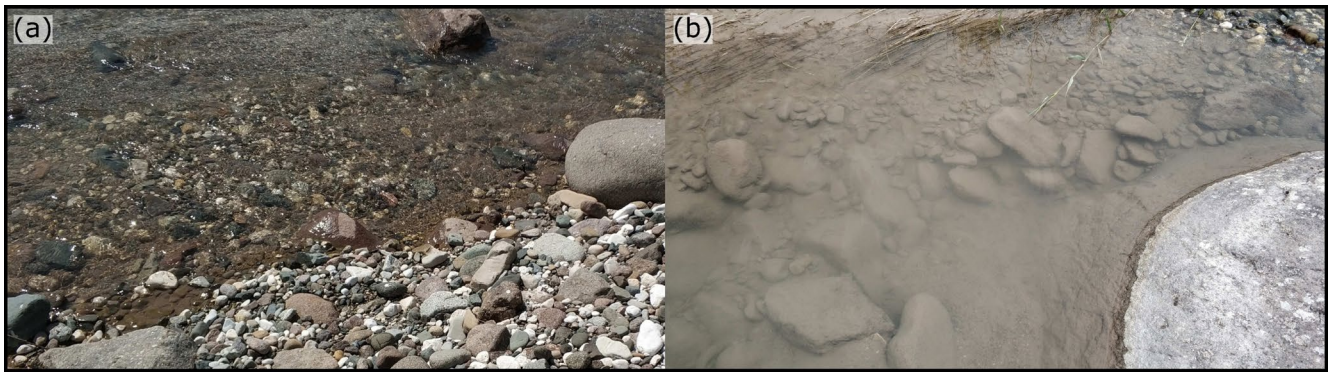

FIGURE 8 | Images of the riverbed in the second sediment sampling site (Figure 1c, located 400 m upstream of P4: (a) before; (b) 1 month after the reservoir flushing.

average, the proportions of gravel and sand exhibited a similar behaviour as observed in POST1, with a further decrease in the percentage of gravel and an increase in the percentage of sand (Table S1 in the Supporting Information). Figure 9 shows a graphical summary of the variation in the gravel, sand and clay distribution.

4.5 | Bedload Initiation Monitoring

Table 5 summarises the observed effects of the flushing on the painted plots deployed to monitor bed load transport. In addition, Figure 10 shows images of the ten painted plots after the flushing, illustrating their appearance and the changes that occurred.

Plot 1, located at the downstream edge of a large partially vegetated gravel bar, was not reached by the water during the flushing. Plot 2, situated slightly upstream on the same bar and a vegetated lateral edge, exhibited signs of partial transport. Similarly, Plot 3, located on the lateral edge of a side bar, experienced partial transport. In Plot 4, positioned on the lateral edge of a gravel side bar, deposition was observed. Plot 5, situated on a side vegetated bar, underwent partial transport and fine sediment deposition. Plot 6, located in the central part of a mid-channel bar, was inundated but no transport was observed after the flushing. Particles of Plot 7, positioned at the upstream edge of the same central bar, were almost entirely transported during the flushing, leaving behind a significant amount of fine sediment. The same situation was observed in Plot 8, located on a mid-channel vegetated bar. On a similar bar in its center, Plot 9 showed mild signs of deposition. Finally, Plot 10, located on a small mid-channel bar, was almost entirely transported by the flushing flows.

Overall, the plots that exhibited the highest gravel mobility were located at the upstream edges of bars immediately downstream of a rapid (7) or a fast-flow unit downstream of a ramp (3, 10). In contrast, no motion was observed in topographically higher regions that were either slightly (6) or not inundated at all (1) during the flushing. Fine sediment deposition was observed on five plots (4, 5, 7, 8, 9), which were situated at the margins of secondary channels (5, 7, 8, 9) or of bars adjacent to a

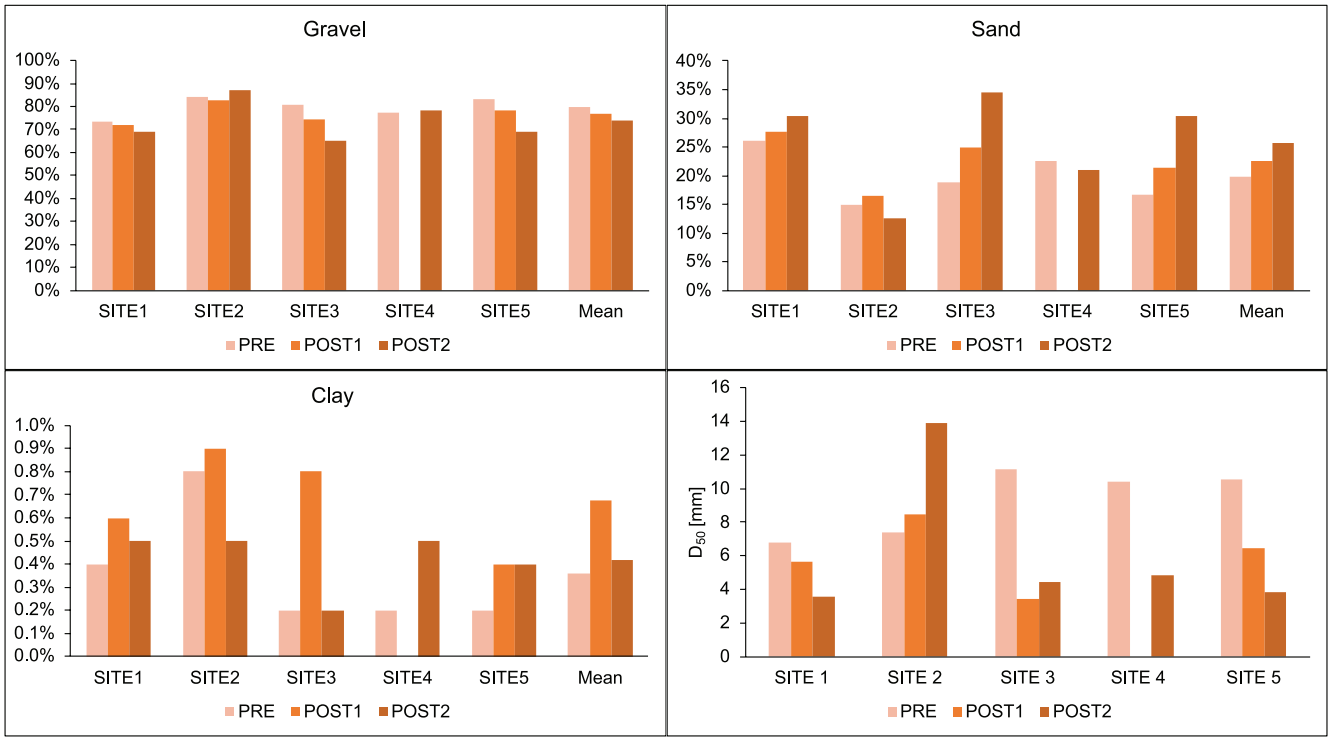

FIGURE 9 | Summary of the bed surface sediment composition in all the sampling sites for the three campaigns. POST1 is taken 1 month after the flushing, and POST2 1 year after the flushing. Top left: variation for the gravel percentage in all the sites in the three campaigns; top right: variation for the sand percentage; bottom left: variation for clay percentage. On the bottom right: D_{50} evolution for all sites.

TABLE 5 | Bed load initiation monitoring: summary of painted gravel plots transport.

Plot n.	Morphological unit	Vegetation cover	Plot location on the bar/unit	Observed sediment transport
1	Mid channel bar	No	Downstream edge	No (above water stage)
2	Mid channel bar	Partial	Lateral edge	Partial transport
3	Side bar	No	Lateral edge	Partial transport
4	Side bar	No	Lateral edge	Fine deposition
5	Right bank	Yes	Lateral edge	Partial transport; fine deposition
6	Mid channel bar	No	Central part	No motion nor deposition
7	Mid channel bar	No	Upstream edge	Partial transport; fine deposition
8	Mid channel bar	Partial	Lateral edge	Partial transport; fine deposition
9	Mid channel bar	Partial	Upstream edge	Fine deposition
10	Mid channel bar	No	Upstream edge	Partial transport

morphological unit with likely low flow velocities (4), typically found just upstream of a weir.

4.6 | Suspended Sediment Dynamics in Natural Floods vs. Reservoir Flushing Events

Discharge and turbidity time series and the related hysteresis patterns are shown in Figures 11 and 12 respectively, for flushing and natural flood events. HI, NS indices and relevant statistical values are presented in Table 6.

The discharge series of natural events exhibit distinct rising and falling limbs, whereas the flushing events do not display discernible discharge trends. Hysteresis loops are more clearly visible for the natural flood events, while the flushing events exhibit noisier patterns. The HI values for both flushing and natural events do not provide sufficient information to distinguish between natural and artificial events. Natural and flushing events instead differ in the average discharge and turbidity values. Although the peak values are of the same order of magnitude, the average values of discharge and turbidity during the flushing event are considerably higher than those of natural events, with average turbidity values up to 20 times higher during flushing events.

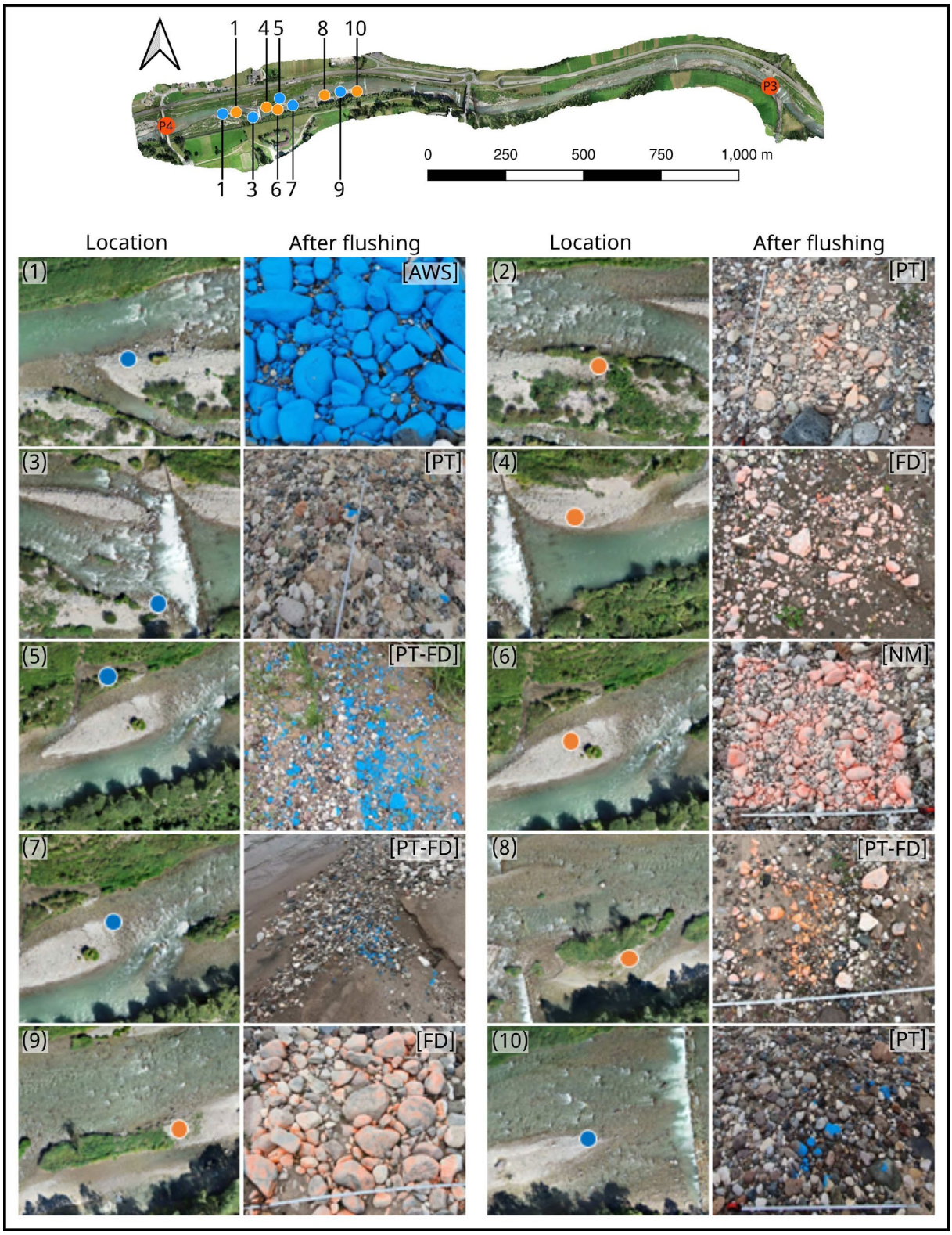

FIGURE 10 | Bed load monitoring. Painted gravel plots: location, conditions after the flushing and type of effects observed (AWS: above water stage; PT: partial transport; NM: no motion nor deposition; FD: fine deposition).

The first stage of the flushing of the Pezzè Reservoir (event 1) and also event 3 display a strong positive NS value (0.81 and 0.40, respectively), indicating an increase in concentration during the rising limb (referred to as the 'flushing' effect), which is caused by the increased concentration levels and is typically related to transport limitations. The second stage of the flushing of the Pezzè reservoir (event 2) exhibited an NS value of −0.06, suggesting a very slight, rather imperceptible trend towards dilution

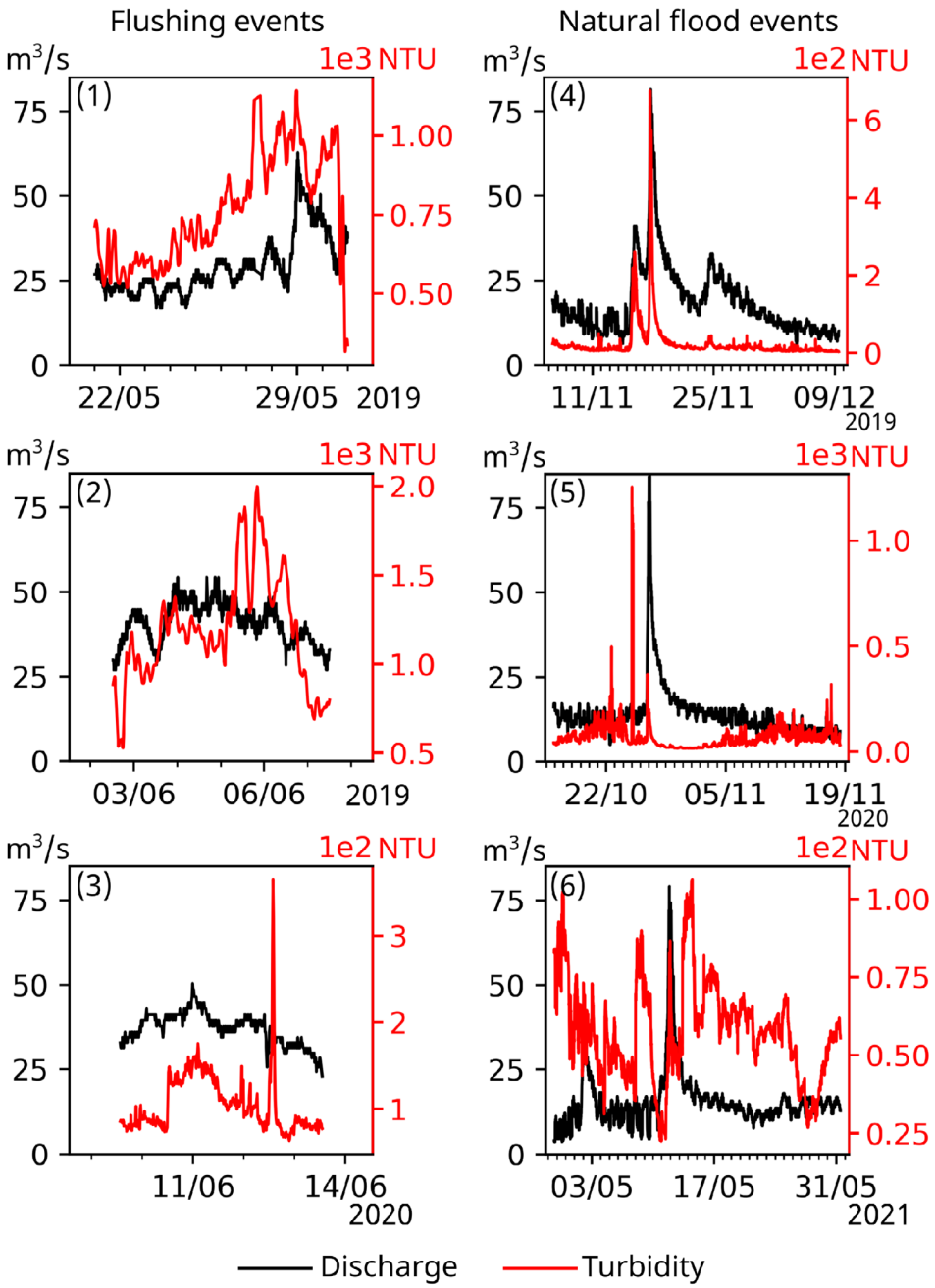

FIGURE 11 | Water discharge and turbidity time series. The left column (subplots 1, 2, 3) shows the Pezzè flushing events 1 and 2 in May–June 2019 and the flushing of the Forte Buso dam in 2020, respectively. The right column (subplots 4, 5, 6) corresponds to natural flood events that occurred in November 2019, between October and November 2020, and in May 2021, respectively.

during this phase, as the NS value approaches 0. Furthermore, flushing event 1 is associated with a positive HI while HI values for flushing events 2 and 3 are weakly negative.

5 | Discussion

5.1 | Spatial Dynamics of Suspended Sediment

In general, the evolution of suspended sediment concentration (SSC) at the monitoring stations 4) shows a gradual decrease in magnitude from the most upstream to the most downstream station. This observed trend is consistent with findings from previous studies on hydraulic sediment flushing, which suggest that sediment transport can be reduced downstream due to local morphological and hydraulic factors (Lepage et al. 2020; Antoine et al. 2020). Two potential mechanisms may explain this pattern: the first is the progressive deposition of suspended sediments due to the combined effects of local channel morphology and hydraulic characteristics, which limit transport capacity relative to the supply rates of flushed sediments. Such processes are commonly observed in systems with significant variations in channel gradient, width, and flow velocity, which can lead to sediment deposition in low-velocity areas (Best and Rhoads 2008; Misset et al. 2019). The second mechanism is the dilution of SSC caused by additional

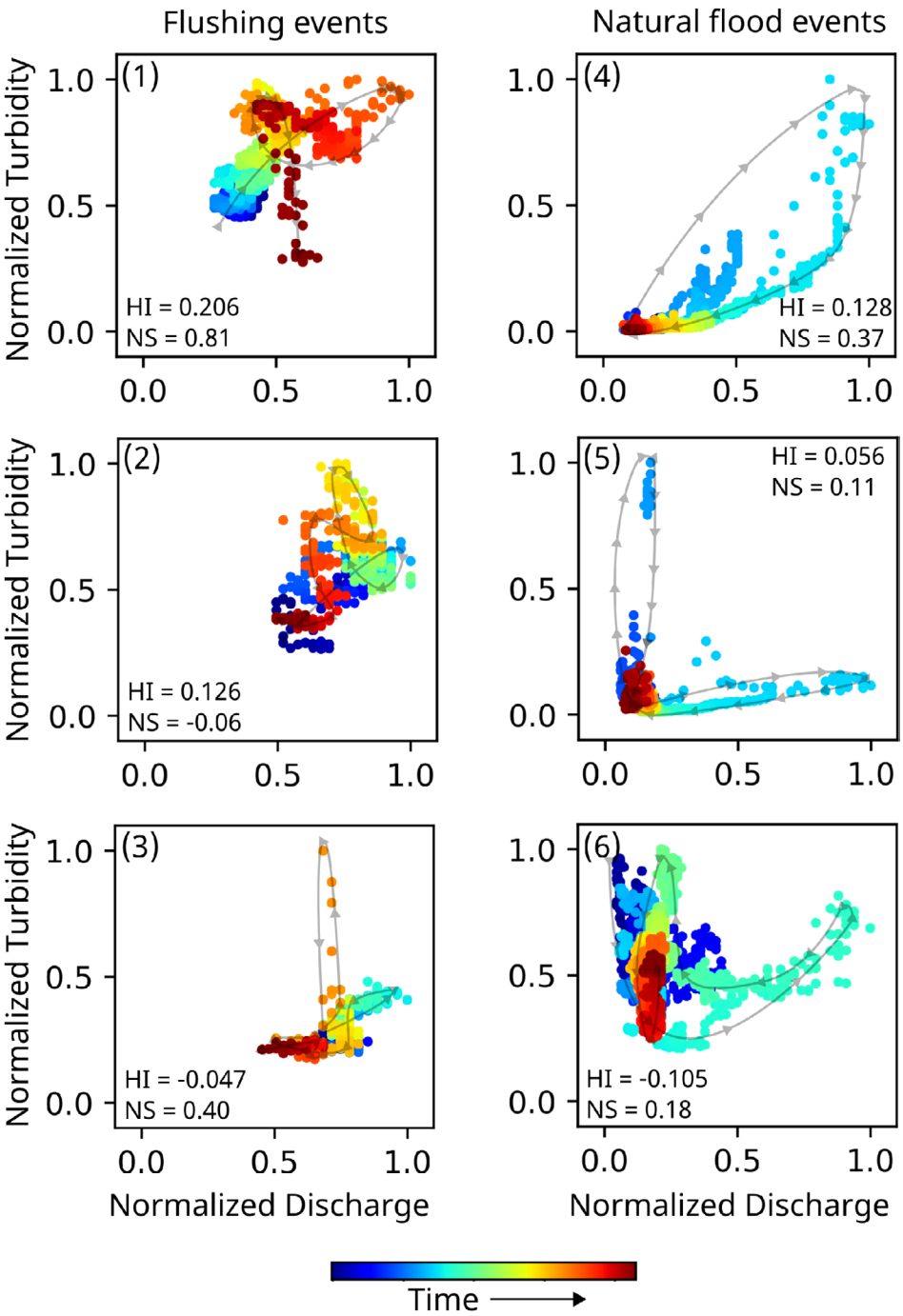

FIGURE 12 | Water discharge—suspended sediment concentration hysteresis patterns. The left column (subplots 1, 2, 3) shows the Pezzè flushing events 1 and 2 in May–June 2019 and the flushing of the Forte Buso dam in 2020, respectively. The right column (subplots 4, 5, 6) corresponds to natural flood events that occurred in November 2019, between October and November 2020, and in May 2021, respectively.

water inputs from lateral tributaries, which is a widely recognised factor influencing sediment concentration in large river systems. In particular, the mixing of tributary water with different sediment concentrations can lead to a decrease in SSC downstream (Nelson et al. 1987).

In particular, the significant differences in SSC values between P1-P2 and P3-P4-P5 suggest the possibility of deposition processes occurring between P2 and P3, in addition to the dilution effect caused by the inlet of the Travignolo stream downstream of P2. However, despite the clear longitudinal decreasing trend, it should be noted that the confidence limits of neighbouring stations (P1-P2 and P3-P4-P5) overlap for a significant portion of the time series, indicating that these differences in SSC between consecutive stations may not have statistical significance for the entire period.

We estimated that approximately 29% of the sediment released from the reservoir (exclusively related to Flushings 1 and 2) were deposited in the first approximately ~9 km downstream

TABLE 6 | Hysteresis comparison between reservoir flushing and natural flood events.

	Event	HI [–]	H. Class [–]	NS [–]	PCC [–]	Duration [h]	Max Q [m^3/s]	Mean Q [m^3/s]	Max T [NTU]	Mean T [NTU]
Reservoir flushing sub-events	1	0.206	2	0.81	0.44	298	62.76	33.42	1142	866
	2	0.126	2	−0.06	−0.38	72	54.35	43.87	1997	1352
	3	−0.047	3	0.40	0.48	85	50.38	37.91	365	108
Natural floods	4	0.128	2	0.37	0.79	429	84.45	24.45	676	36
	5	0.056	1	0.11	0.01	600	86.67	14.86	1253	64
	6	−0.105	4	0.18	−0.06	119	79.15	27.49	107	60

Abbreviations: H. class, hysteresis class; HI, hysteresis index; NS, normalised slope; PCC, Pearson's correlation coefficient; Q, water discharge; T, water turbidity.

of the dam, between stations P1 and P2. Moreover, approximately 38% of the sediment deposited in the subsequent 10 km upstream of station P3, while 12% of the sediment deposited between P3 and P4, and P4 and P5 in equal proportions (Figure 3), despite the P4-P5 reach being longer than the P3-P4 reach (3.8 km compared to 2.1 km). The differences in transported sediment between the upstream (P1-P2 and P2-P3) and downstream (P3-P4 and P4-P5) reaches cannot be easily inferred solely from their morphological properties. The upstream reaches are narrower and steeper, whereas the downstream reaches are wider, less steep, and have higher flow rates (Figure 2, and Table 2). Additionally, although Flushing 1 lasted for 15 days and Flushing 2 just over 5 days, the sediment loads passing through each station during the two events were relatively similar. This can be attributed to the higher flow rates during Flushing 2 (Figure 2) which maintained similar SSC values (Figure 4). In addition, sediment deposited on the riverbed during Flushing 1 may have been resuspended and transported downstream during Flushing 2.

The analysis of local mass balances (Table 4 and Figure 5) during the intermediate phases, Washing 1 and 2, indicates that the recorded SSC and the associated sediment loads are to be attributed to the entrainment of sediment deposited in the reach during the previous flushing phases (Tena et al. 2014). In fact, during washing periods, sediment release from the dam was minimised, while sediment contributions from lateral tributaries can be considered negligible due to the lack of rainfall events. The hypothesis that the source of SSC during washing phases is the riverbed deposited sediment is supported by findings in Figure 7, where the negative trend during Washing 1 suggests dominant sediment entrainment, whereas the succession of positive and negative trends in Washing 2 implies a progressive depletion of sediment from upstream, allowing the flow to entrain additional sediment present in the reach.

In summary, based on our findings, we speculate that the high sedimentation rates observed in reaches P1-P2 and P2-P3 result from the high SSC exceeding the sediment transport capacity of the flow. This is supported by the generally good agreement between the trends shown by the relative theoretical transport capacity and measured transport in all subreachs (Figure 6). Once the excess sediment was deposited in the two upstream reaches (P1 to P3), the remaining sediment available for transport by the flow between P3 and P5 likely approached the theoretical transport capacity, which could explain the lower net deposition in these reaches.

The initial amount of fine sediment available for transport in the river bed was not quantified in this study and may contribute to the reach-scale sediment budget (Tena et al. 2012). However, the relatively high frequency of flushing events of the Pezzè reservoir (one every 3–4 years) might have built sediment deposits that have not been completely removed before the studied flushing, and which might have become additional sediment sources, as observed in similar studies (Antoine et al. 2020; Bulteau et al. 2024). These assumptions also find support from the lack of rainfall events during the flushing period, which reinforces the assumption of a minor role for the lateral tributaries, with the exception of San Pellegrino and Travignolo.

Furthermore, the SSC during flushing in the main channel of the Avisio is consistently 2–3 times higher than the SSC associated with natural flood events (Figure 12). Although most of the local mass balances between stations P3 and P4 were not statistically significant, the trends observed in Sections 4.4 and 4.5 further support the hypothesised suspended sediment dynamics. Considering that the discharge in the natural tributaries is significantly lower than the discharge in the main channel of the Avisio, neglecting their suspended sediment contributions in the developed sediment budget appears to be justified. These assumptions may introduce some uncertainties, which should be considered in future studies to provide a more comprehensive understanding of the reach-scale sediment dynamics.

Finally, it is important to highlight that the 2019 flushing, influenced by the extraordinary material input from Storm Vaia, not only lasted longer than previous events but also resulted in exceptionally high sediment release. Unlike earlier flushings, which typically lasted about 10 days, the 2019 operation extended over 21 days, indicating an increased sediment load requiring a more extended mobilisation period. This significant increase in suspended material, estimated at roughly 400 000 tons, underscores the substantial impact of the Vaia storm on sediment availability in the system (Rainato et al. 2021).

5.1.1 | Uncertainty of Suspended Sediment Loads

Overall, the uncertainty analysis in this study resulted in an average uncertainty value of 23.5%. It was found that 5 out of 16 (approximately 30%) of the local mass balances computed were statistically significant. This percentage is comparable to a previous study by Antoine et al. (2020), which focused on SSC uncertainty during reservoir flushing in Alpine rivers and found that only 14 out of 52 sediment budgets (approximately 26%) had statistical significance. However, despite their low statistical significance, the results on the mass balances in the P3-P4 reach were justified with the support of field observations.

In this study, we acknowledged several minor sources of uncertainty that were not fully quantified, including the flow contribution from catchment areas between stations ($\sim 250\ km^2$, excluding major tributaries). This could include additional water from snowmelt runoff and increased local SSC from tributaries. Although no rainfall events were recorded during the flushing event, rising temperatures in the region could have accelerated snowmelt, potentially influencing SSC (Tena et al. 2012). Models like the one proposed by Turowski et al. (2010) can estimate long-term suspended sediment loads based on catchment size, but their use for time-series estimation of tributary inputs in the Avisio River is limited due to the unavailability of discharge data for the tributaries. While GIS-based methods and catchment models could provide rough estimates of tributary sediment load, contributions from these tributaries are generally small compared to the main discharge at Avisio. The Travignolo, whose contribution was accounted for, is the main exception, as the other tributaries are primarily active during natural events, which did not occur in the study period. Given the significantly higher sediment release during flushing events compared to natural sediment supply, neglecting tributary contributions does not notably affect the results.

The uncertainties associated with the SSC-NTU relationships derived from manually collected and analysed water samples represent the largest quantified source of uncertainty in this study. A more comprehensive sample collection strategy covering the entire range of SSC during different stages of the flushing event would help reduce uncertainties. The use of automatic samplers could also be considered to improve data collection.

5.2 | Bed Surface Sediment Composition and Bedload Initiation

The reduction of the gravel percentage and the increase in sand and clay fractions between pre-flushing (PRE) and 1 month after the flushing (POST1) samples indicate that the deposited fine sediment from the reservoir were still present on the riverbed. Additionally, 1 year after the flushing (POST2), the riverbed composition had only partially recovered from the effects of the deposition. In all the sites, except for site 2, the mean diameter D_{50} 1 year after the flushing was still smaller than the one calculated before the flushing. The increase in the sand fraction between POST1 and POST2 in site 5, and the parallel decrease in D_{50}, further suggests that sediment deposits from the first 17 km during the flushing may have been resuspended and partially transported downstream to the P4-P5 subreach. This persistence of fine sediment can have ecological implications, such as altering the physicochemical and thermal conditions of aquatic habitats, hydraulic conductivity and dynamics of hyporheic flows (Boano et al. 2014) and affecting oxygen and nutrient exchange, as well as hindering the movement of invertebrates into deeper sediment regions (Brunke and Gonser 1997; Wharton et al. 2017).

The dynamics of fine sediment removal appear to be influenced by spatial heterogeneity associated with bed topography, flow patterns and inundation dynamics resulting from variability at the spatial scale of Hydro-Morphological Units (HMU, sensu Belletti et al. 2017). Site 4, located below a weir that creates a highly turbulent flow pattern, showed a clear reduction in the fine sediment fraction one year after the flushing. Site 2, located on a small side bar prone to inundation, showed a slight reduction in the fine fraction. However, in sites 1, 3 and 5, the fine sediment fraction remained almost unchanged after one year and was higher compared to pre-flushing conditions. These sites are located in hydro-morphological units likely to experience low value of the near-bed shear stress, which limits sediment entrainment. Site 1 is on a side bar of a secondary channel, while sites 3 and 5 are located on (point) bars within gentle bends of the main channel. The presence of fine sediment deposition on the riverbed is also visible in most of the sites where painted gravel plots were established. Sites located near secondary and backwater channels or surrounded by vegetation (Table 5) showed signs of deposition, indicating the incidence of high rates of fine sediment deposition from the reservoir throughout the reach (Sections 4.1 and 4.4). The deposition near secondary channels (site 7) and vegetated areas (sites 2, 8, 9) can be attributed to the reduction in flow velocity caused by the presence of vegetation, which hindered the complete removal of deposited sediment by the washing flows.

Although the painted gravel plots do not provide a quantification of bedload transport rates, they offer valuable insights into the spatial variability of bedload occurrence during the flushing flows. None of the plots were completely removed, and in cases where gravel was moved, it was often found a few meters downstream, indicating relatively short travel distances for the transported gravel and cobbles. These observations suggest the occurrence of, thought to a limited extent, coarse sediment mobility during the entire 28-days long flushing event.

These findings on bedload initiation provide important information for the modelling of flushing flows, which has been rather scarce so far. The flushing in the Avisio River was able to transport both fine and coarse sediment fractions, with the fine fraction being predominantly in suspension. However, the mobilisation of coarse riverbed sediment likely occurred in faster-flowing areas of the channels, where direct measurements were not possible. To gain further insight into sediment dynamics during flushing operations in the Avisio and other Alpine rivers, hydraulic models that account for the mobility of both fine and coarse sediment fractions should be employed. These models should consider the size-selective partial mobility conditions and the transport of fines and coarse sediment simultaneously (Kuhnle et al. 2013; Stradiotti et al. 2020; Tavelli et al. 2020).

5.3 | Suspended Sediment Dynamics in Natural Floods Versus Reservoir Flushing Events

In general, hysteresis patterns are not clearly identified in flushing events (Figure 12). However, despite the noisy patterns, the hysteresis analysis can still provide insights on the dynamics in place. The positive HI value for flushing event 1 would indicate that the peak concentration occurred ahead of the peak discharge, whereas the weakly negative HI values for flushing events 2 and 3 are related to slightly counterclockwise loops in which the concentration values on the falling limb are higher than those on the rising limb. The mean and maximum turbidity of flushing event 2 was approximately 1.65 times higher compared to flushing event 1. Although difficult to quantify, this supports our hypothesis of sediment resuspension during flushing event 2. Overall, compared to natural events, flushing events exhibit a poorer correlation between turbidity and discharge series (Figure 11), responsible for the noisier behaviour discussed in hysteresis patterns, confirming previous findings (Vericat and Batalla 2006; Tena et al. 2014). The disconnection between discharge and turbidity in flushing events may be related to several concurring factors. One is the attenuation of the main flushing signal, released 18 km upstream of the measuring station P4 in events 1 and 2. Moreover, the dilution effect produced in P4 by the combination of the flushing flows with relatively high seasonal discharges (San Pellegrino and Travignolo diluting the Avisio flushing signal in the case of events 1 and 2, and San Pellegrino and Avisio diluting the Travignolo flushing signal in the case of event 3). Another factor is the shape of the flushing discharge time series, characterised by multiple oscillations without a dominant peak, unlike a natural event. A fourth factor is related to the different balancing between sediment supply and transport capacity limitation in the two types of events (Vercruysse et al. 2017). In natural floods, sediment entrainment is a gradual process, involving sediment from the riverbed and banks, entering the flow as the event increases its energy and duration. The availability of sediment for transport during natural floods can be influenced by the time elapsed since the previous flushing event, and since natural flood events mobilise sediment upstream of the study reach. This gradual process contrasts with the dynamics of a flushing event, where the sudden release of a large volume of sediment from the reservoir, often associated with abrupt bulk detachments, can cause a rapid increase in turbidity. Unlike natural flood events, where SSC is typically supply-limited, flushing-induced sediment transport may become more capacity-limited, leading to a disconnect between the flushing flow magnitude and SSC dynamics (Espa et al. 2019; Tarekegn et al. 2014). Such flushing events can exhibit chaotic sediment behaviour, as the mobilised fine sediments are transported differently compared to their natural counterparts (Espa et al. 2019).

This is further reflected in the turbidity series characteristics. In one natural event (event 5), the peak turbidity magnitude is comparable to the peaks observed during the flushing events (Tena et al. 2014), suggesting that the resuspension of sediment deposited during the previous flushing might have contributed to the elevated turbidity levels. That said, natural floods are characterised, in most cases, by a single turbidity peak that is considerably higher than their average turbidity levels. For the considered events, the peak-to-average turbidity ratio (Max T/Mean T) is equal to 1.32, 1.48 and 3.38 for flushing events 1, 2 and 3, respectively, and equal to 18.78, 19.58 and 1.78 for the natural floods events 4, 5 and 6, respectively. Notably, the average turbidity levels during the reservoir flushing were up to 2000% higher compared to natural floods, while the average duration of the flushing events was only about 35% of the duration of natural floods (Table 6). Both the duration of exposure and the high turbidity levels have been associated with negative effects on fish populations (Newcombe and Jensen 1996), highlighting an important difference between artificial and natural events in terms of their potential impacts on the aquatic ecosystem.

Despite showing clearer patterns, however, the hysteresis indices for natural events do not show coherent behaviour among them. Event 4 was the first natural event that occurred 6 months after the flushing analysed in this study. The positive NS value observed during the event indicates a flushing effect in the rising limb, suggesting transport limitations and the presence of abundant sources of suspended sediment upstream. This behaviour could be attributed to the resuspension of sediment that were deposited during the reservoir flushing (Tena et al. 2014). The strong correlation between SSC and discharge observed during the washing periods of the reservoir flushing (Figure 7) supports the hypothesis that a significant amount of fine sediment, likely deposited during previous flushing events, could have been present in the riverbed before and during this storm event. Event 5 shows similar characteristics to Event 4, as it occurred 5 months after the flushing event in the Travignolo tributary (Event 3), ~2 km upstream of the confluence with the Avisio River. The higher turbidity levels observed in this event may be then attributed to the resuspension of sediment trapped in the reach directly upstream of the measurement station. Contrary to events 4 and 5, however, event 6 features a counterclockwise hysteresis loop, associated with a peak in discharge preceding the peak in turbidity, which typically indicates that the flood wave propagates faster than the sediment wave. This pattern is often observed when sediment is sourced from distant locations or through bed and bank erosion (Petts et al. 1985; Gilvear and Petts 1985). In the case of flushing event 3, although rather noisy, the counterclockwise behaviour reflects the time lag between the discharge and sediment waves. However, in natural event 6, this counterclockwise behaviour is likely associated with fine sediment entrainment from the riverbed. Since this event occurred in May–June, 2021 and was not preceded by any flushing event, the lower turbidity peak suggests that the sediment sources were limited compared to the flushing events.

The seasonality of the natural events could further contribute to the differences observed (Lenzi et al. 2003). Flow and sediment dynamics in rivers can vary significantly depending on the season, with factors such as snowmelt, rainfall patterns and vegetation growth playing important roles (López-Tarazón and Batalla 2014; Tena et al. 2014; Vercruysse et al. 2017). For instance, events 4 and 5 occurred in October and November (autumn), thus the reduced vegetation cover likely increased hillslope erosion, leading to a delayed supply of sediment and a retarded SSC peak, and resulting in a counterclockwise hysteresis loop. Event 6, measured in May (spring) occurred when vegetated hillslopes played a smaller role, and sediment transport

was primarily driven by channel erosion, causing an anticipated SSC peak and a clockwise loop. To fully understand the seasonal variations and their influence on sediment dynamics, a longer series of flood events spanning multiple seasons would be necessary. This would allow for a more comprehensive analysis of the hydrological and sedimentary processes occurring in the river throughout the year.

5.4 | Observations for Future Management Strategies

The analysis reveals that the great majority of the flushed sediment (79%) is deposited along the downstream river segment, in agreement with previously studied flushing (e.g., Espa et al. 2016; Antoine et al. 2020), where up to 80% of the estimated total mass of sediment flushed was trapped within the study sites. More specifically, in this work, we estimated the distribution of flushed sediment as follows: 29% deposited between P1 and P2 (~485 channel widths), 38% between P2 and P3 (~620 channel widths), 6% between P3 and P4 (~88 channel widths) and 6.3% between P4 and P5 (~110 channel widths). Fine sediment accumulation in the riverbed is of ecological concern (Wohl and Cenderelli 2000; Espa et al. 2016), and its mitigation, during or after the flushing, is considered with high attention among the management priorities of flushing operations.

The SS dynamics observed during the washing periods analysed in this study show their potential to mitigate the deposition problem. In particular, in subreach P3–P4, during Washing event 1, it was estimated that approximately 20% of the sediment deposited after Flushing event 1 was removed in just 3 days. This is of high management interest, as clear water releases (or washing, in this manuscript) are not a common practice within the flushing programmes, and, to our knowledge, it has not been reported in other published reservoir flushing studies, at least in the Italian Alps.

Figure 13 shows the evolution of the sediment balance between P3 and P4 until the end of the Washing event 1 (cumulative difference in passing sediment mass). An increasing sediment balance trend suggests a dominant deposition process, while a decreasing balance suggests erosion or resuspension. It can be hypothesized that if the observed relationship between SSC and water discharge can hold for hypothetically longer periods of washing, then, extending the duration of washings can potentially remove a larger amount of deposited sediment during the flushing. This hypothesis assumes an infinite sediment availability and the validity of the same SSC–discharge relationship, which may not hold over longer washing periods as the sediment source would gradually deplete. Additionally, the feasibility of implementing such schemes, including the capacity of the dam to sustain extended discharges, needs to be assessed, considering that the average discharge would not be able to reach sediment deposits that might have built during preceding higher flushing discharges. The increase of fine sediment in the granulometric curves even 1 year after the flushing can support this statement. Furthermore, the specific characteristics of each river and reservoir system, such as channel morphology, sediment inputs, flushing frequency and technical and economic constraints, need to be carefully considered. Nevertheless, this suggests possibilities for more environmentally friendly implementation of reservoir flushing, where the adverse ecological effects of fine sediment deposition can be mitigated to a great extent.

Further research is needed to understand the ecological implications of dam flushing and the effects on local biota. This includes studying the impacts of increased SSC and flows on the river ecosystem and assessing the response of different organisms to these changes. Additionally, exploring alternative flushing management strategies, such as shorter but more frequent flushing events that mimic natural sediment regimes, or synchronising flushing operations with natural floods, could provide valuable insights for sustainable sediment management in river systems (e.g., Folegot et al. 2021).

6 | Conclusions

Sediment flushing has been proven an effective measurement to take on reservoir siltation, notwithstanding, it can cause severe effects on downstream ecosystems. In this study, a comprehensive monitoring program was established to understand the sediment dynamics during reservoir flushing operations and to quantify the effects at different spatial and temporal scales along a 30 km river segment. High rates of deposition and fine sediment bulks were observed along the study segment.

An uncertainty propagation model was proposed to estimate the significance of local mass balances between neighbouring stations. A global uncertainty value of 23.5% was determined, for which 5 out of the 16 local mass balances obtained in this study were significant. Grain size distributions show a substantial reduction of the median particle size after the flushing, with small

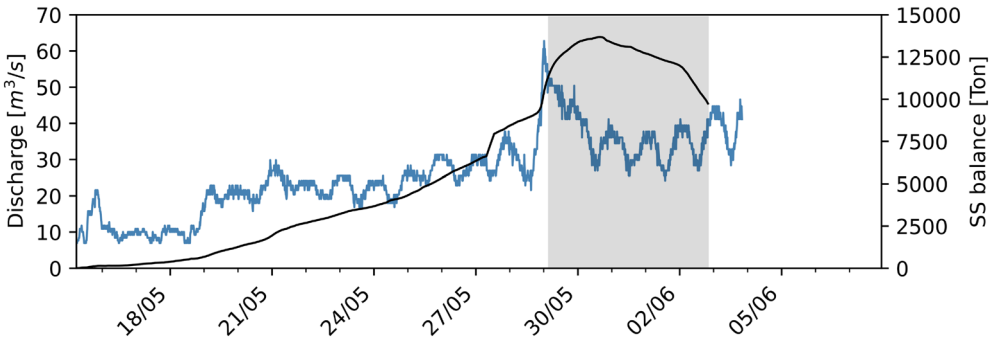

FIGURE 13 | Discharge (blue line) and sediment budget (black line) time series for the subreach P3-P4. The washing period is highlighted in grey.

recovery rates after one year. Albeit the flushings were performed during the spring season, when average flows are higher as a result of snowmelt runoff, the river was not able to entirely transport the sediment-loaded flushing flows.

We compared the suspended sediment dynamics during reservoir flushing versus those in natural storm events. Natural floods in this study exhibited well-defined flow-concentration relationships; however, there was little consistency in the direction and behaviour of hysteresis loops. In contrast, we evidenced a strong disconnection between sediment concentration and discharge during reservoir flushing operations. We hypothesise that the unpredictability of suspended sediment dynamics during reservoir flushing can be related to the complex scouring processes inside the reservoir. More extensive field evidence is needed to prove this theory.

We also quantified how much an off-the-schedule, temporary interruption of the flushing operations in favour of releasing clear water pulses can remove deposited sediment during the previous flushing. Based on these results, we suggest considering alternating flushing flows and washing flows, for which in-stream deposition can be mitigated, though the feasibility of such a strategy will require careful, site-specific assessments. These findings contribute to the development of more environmentally sensitive sediment management strategies, but further research and detailed analysis are required to refine and validate these approaches.

Acknowledgements

The work was carried out under the HyMoCARES project, within the EU Interreg Alpine Space programme. It has also been supported by the Italian Ministry of Universities and Research (MUR), in the framework of the project DICAM-EXC (Departments of Excellence 2023-2027, grant L232/2016) and by the European Union under NextGeneration EU. PRIN 2022 'SEDMORNET' Prot. n. E53D23004200006. Finally, to Servizio Bacini montani, APPA Trento and Vigili del Fuoco for their contribution to this work. This manuscript reflects only the Authors' views and opinions; neither the European Union nor the European Commission can be considered responsible for them. Open access publishing facilitated by Universita degli Studi di Trento, as part of the Wiley - CRUI-CARE agreement.

Conflicts of Interest

The authors declare no conflicts of interest.

Data Availability Statement

The data that support the findings of this study are available from the corresponding author upon reasonable request.

Endnotes

[1] http://www.floods.it.

[2] https://siat.provincia.tn.it/stem/.

References

Antoine, G., B. Camenen, M. Jodeau, J. Némery, and M. Esteves. 2020. "Downstream Erosion and Deposition Dynamics of Fine Suspended Sediments due to Dam Flushing." *Journal of Hydrology* 585: 124763. https://doi.org/10.1016/j.jhydrol.2020.124763.

Auel, C., and R. M. Boes. 2011. "Sediment Bypass Tunnel Design–Review and Outlook." *Dams and Reservoirs Under Changing Challenges* 40312.

Baoligao, B., F. Xu, X. Chen, X. Wang, and W. Chen. 2016. "Acute Impacts of Reservoir Sediment Flushing on Fishes in the Yellow River." *Journal of Hydro-Environment Research* 13: 26–35. https://doi.org/10.1016/j.jher.2015.11.003.

Belletti, B., C. de Garcia Leaniz, J. Jones, et al. 2020. "More Than One Million Barriers Fragment Europe's Rivers." *Nature* 588, no. 7838: 436–441. https://doi.org/10.1038/s41586-020-3005-2.

Belletti, B., M. Rinaldi, M. Bussettini, et al. 2017. "Characterising Physical Habitats and Fluvial Hydromorphology: A New System for the Survey and Classification of River Geomorphic Units." *Geomorphology* 283, no. 4: 143–157. https://doi.org/10.1016/J.GEOMORPH.2017.01.032 https://www.sciencedirect.com/science/article/pii/S0169555X16305852.

Bergamin, F. 2017. "Studio dell'evoluzione morfologica del fiume adige nell'ultimo secolo: analisi di sezioni storiche e modello interpretativo".

Best, J. L., and B. L. Rhoads. 2008. "Sediment Transport, Bed Morphology and the Sedimentology of River Channel Confluences." In *River Confluences, Tributaries and the Fluvial Network*, 45–72. John Wiley & Sons, Ltd.

Bilotta, G., N. Burnside, L. Cheek, et al. 2012. "Developing Environment-Specific Water Quality Guidelines for Suspended Particulate Matter." *Water Research* 46, no. 7: 2324–2332. https://doi.org/10.1016/j.watres.2012.01.055.

Blott, S. J., and K. Pye. 2012. "Particle Size Scales and Classification of Sediment Types Based on Particle Size Distributions: Review and Recommended Procedures." *Sedimentology* 59: 2071–2096. https://doi.org/10.1111/j.1365-3091.2012.01335.x.

Boano, F., J. W. Harvey, A. Marion, et al. 2014. "Hyporheic Flow and Transport Processes: Mechanisms, Models, and Biogeochemical Implications." *Reviews of Geophysics* 52: 603–679. https://doi.org/10.1002/2012RG000417.

Boretto, G., S. Crema, L. Marchi, G. Monegato, L. Arziliero, and M. Cavalli. 2021. "Assessing the Effect of the Vaia Storm on Sediment Source Areas and Connectivity Storm in the Liera Catchment (Dolomites)." In *Egu General Assembly Conference Abstracts*, EGU21–7643. Copernicus Publications.

Brandt, S. A. 2000. "Prediction of Downstream Geomorphological Changes After Dam Construction: A Stream Power Approach." *International Journal of Water Resources Development* 16: 343–367. https://doi.org/10.1080/713672510.

Brandt, S. A., and J. Swenning. 1999. "Sedimentological and Geomorphological Effects of Reservoir Flushing: The cachí Reservoir, Costa Rica, 1996." *Geografiska Annaler. Series A, Physical Geography* 81, no. 3: 391–407. https://doi.org/10.1111/j.0435-3676.1999.00069.x.

Brunke, M., and T. Gonser. 1997. "The Ecological Significance of Exchange Processes Between Rivers and Groundwater." *Freshwater Biology* 37, no. 1: 1–33. https://doi.org/10.1046/j.1365-2427.1997.00143.x.

Bulteau, T., B. Marteau, R. J. Batalla, E. Chapron, P. Valette, and H. Piégay. 2024. "Effects of Repeated Drawdown Flushing on Riverbed Fine Sediment Dynamics Downstream From a Dam." *Anthropocene* 47: 100444.

Camenen, B., G. Dramais, A. Buffet, et al. 2018. "Estimation of Sand Suspension in a Secondary Channel of an Alpine River." *E3S Web of Conferences* 40: 04014. https://doi.org/10.1051/e3sconf/20184004014.

Carolli, M., C. G. de Leaniz, J. Jones, et al. 2023. "Impacts of Existing and Planned Hydropower Dams on River Fragmentation in the Balkan

Region." *Science of the Total Environment* 871: 161940. https://doi.org/10.1016/j.scitotenv.2023.161940.

Chanson, H. 2004. "11–Sediment Transport Mechanisms: 2. Suspended-Load Transport." In *Hydraulics of Open Channel Flow (Second Edition)*, edited by H. Chanson, 2nd ed., 204–217. Butterworth-Heinemann. https://doi.org/10.1016/B978-075065978-9/50017-9.

Chow, V. T. 1954. *Open-Channel Hydraulics*. McGraw Hill Book Company, Inc.

Chung, S. W., I. H. Ko, and Y. K. Kim. 2008. "Effect of Reservoir Flushing on Downstream River Water Quality." *Journal of Environmental Management* 86, no. 1: 139–147. https://www.sciencedirect.com/science/article/pii/S0301479706003847. https://doi.org/10.1016/J.JENVMAN.2006.11.031.

Church, M., and M. Hassan. 1992. "Size and Distance of Travel of Unconstrained Clasts on a Streambed." *Water Resources Research* 28, no. 1: 299–303.

Crosa, G., E. Castelli, G. Gentili, and P. Espa. 2010. "Effects of Suspended Sediments From Reservoir Flushing on Fish and Macroinvertebrates in an Alpine Stream." *Aquatic Sciences* 72: 85–95. https://doi.org/10.1007/s00027-009-0117-z.

Davies-Colley, R., and D. Smith. 2001. "Turbidity Suspenied Sediment, and Water Clarity: A Review 1." *JAWRA Journal of the American Water Resources Association* 37, no. 5: 1085–1101.

Di Baldassarre, G., and A. Montanari. 2009. "Uncertainty in River Discharge Observations: A Quantitative Analysis." *Hydrology and Earth System Sciences* 13, no. 6: 913–921.

Druine, F., R. Verney, J. Deloffre, et al. 2018. "In Situ High Frequency Long Term Measurements of Suspended Sediment Concentration in Turbid Estuarine System (Seine Estuary, France): Optical Turbidity Sensors Response to Suspended Sediment Characteristics." *Marine Geology* 400, no. 6: 24–37. https://doi.org/10.1016/j.margeo.2018.03.003.

Eaton, A., M. Franson, and Association, A. P. H., Association, A. W. W., & Federation, W. E. 2005. *Standard Methods for the Examination of Water and Wastewater*. American Public Health Association.

Espa, P., R. J. Batalla, M. L. Brignoli, G. Crosa, G. Gentili, and S. Quadroni. 2019. "Tackling Reservoir Siltation by Controlled Sediment Flushing: Impact on Downstream Fauna and Related Management Issues." *PLoS One* 14, no. 6: e0218822. https://doi.org/10.1371/journal.pone.0218822.

Espa, P., M. L. Brignoli, G. Crosa, G. Gentili, and S. Quadroni. 2016. "Controlled Sediment Flushing at the Cancano Reservoir (Italian Alps): Management of the Operation and Downstream Environmental Impact." *Journal of Environmental Management* 182: 1–12. https://doi.org/10.1016/j.jenvman.2016.07.021.

Espa, P., E. Castelli, G. Crosa, and G. Gentili. 2013. "Environmental Effects of Storage Preservation Practices: Controlled Flushing of Fine Sediment From a Small Hydropower Reservoir." *Environmental Management* 52: 261–276. https://doi.org/10.1007/s00267-013-0090-0.

Folegot, S., M. C. Bruno, S. Larsen, et al. 2021. "The Effects of a Sediment Flushing on Alpine Macroinvertebrate Communities." *Hydrobiologia* 848: 3921–3941. https://doi.org/10.1007/s10750-021-04608-8.

Gilvear, D. J., and G. E. Petts. 1985. "Turbidity and Suspended Solids Variations Downstream of a Regulating Reservoir." *Earth Surface Processes and Landforms* 10: 363–373. https://doi.org/10.1002/esp.3290100408.

Godsey, S. E., J. W. Kirchner, and D. W. Clow. 2008. "Concentration–Discharge Relationships Reflect Chemostatic Characteristics of US Catchments." *Hydrological Processes* 23, no. 23: 1644–1844.

Grimardias, D., J. Guillard, and F. Cattanéo. 2017. "Drawdown Flushing of a Hydroelectric Reservoir on the rhône River: Impacts on the Fish Community and Implications for the Sediment Management." *Journal of Environmental Management* 197, no. 7: 239–249. https://doi.org/10.1016/J.JENVMAN.2017.03.096 https://www.sciencedirect.com/science/article/pii/S0301479717303213.

ICOLD. 2009. *Sedimentation and Sustainable Use of Reservoirs and River Systems (Bulletin)*. International Commission On Large Dams.

Kjelland, M. E., C. M. Woodley, T. M. Swannack, and D. L. Smith. 2015. "A Review of the Potential Effects of Suspended Sediment on Fishes: Potential Dredging-Related Physiological, Behavioral, and Transgenerational Implications." *Environment Systems and Decisions* 35, no. 9: 334–350. https://doi.org/10.1007/s10669-015-9557-2.

Kondolf, G. M. 1997. "Hungry Water: Effects of Dams and Gravel Mining on River Channels." *Environmental Management* 21, no. 4: 533–551. https://doi.org/10.1007/s002679900048.

Kondolf, G. M., and A. Farahani. 2018. "Sustainably Managing Reservoir Storage: Ancient Roots of a Modern Challenge." *Watermark* 10, no. 2: 117.

Kondolf, G. M., Y. Gao, G. W. Annandale, et al. 2014. "Sustainable Sediment Management in Reservoirs and Regulated Rivers: Experiences From Five Continents." *Earth's Future* 2, no. 5: 256–280. https://doi.org/10.1002/2013ef000184.

Ku, H. H. 1966. "Notes on the Use of Propagation of Error Formulas." *Journal of Research of the National Bureau of Standards* 70, no. 4: 263–273.

Kuhnle, R. A., M. Asce, D. G. Wren, et al. 2013. "Sand Transport Over an Immobile Gravel Substrate." *Journal of Hydraulic Engineering* 139: 167–176. https://doi.org/10.1061/(ASCE)HY.1943-7900.

Le Coz, J., B. Renard, L. Bonnifait, F. Branger, and R. Le Boursicaud. 2014. "Combining Hydraulic Knowledge and Uncertain Gaugings in the Estimation of Hydrometric Rating Curves: A Bayesian Approach." *Journal of Hydrology* 509: 573–587.

Legout, C., I. Droppo, J. Coutaz, C. Bel, and M. Jodeau. 2018. "Assessment of Erosion and Settling Properties of Fine Sediments Stored in Cobble Bed Rivers: The Arc and isère Alpine Rivers Before and After Reservoir Flushing." *Earth Surface Processes and Landforms* 43, no. 6: 1295–1309. https://doi.org/10.1002/esp.4314.

Lenzi, M. A., L. Mao, and F. Comiti. 2003. "Interannual Variation of Suspended Sediment Load and Sediment Yield in an Alpine Catchment." *Hydrological Sciences Journal* 48, no. 6: 899–915.

Lepage, H., M. Launay, J. LeCoz, et al. 2020. "Impact of Dam Flushing Operations on Sediment Dynamics and Quality in the Upper rhône River, France." *Journal of Environmental Management* 255: 109886. https://doi.org/10.1016/j.jenvman.2019.109886.

López-Tarazón, J. A., and R. J. Batalla. 2014. "Dominant Discharges for Suspended Sediment Transport in a Highly Active Pyrenean River." *Journal of Soils and Sediments* 14: 2019–2030.

Mao, L., and N. Surian. 2010. "Observations on Sediment Mobility in a Large Gravel-Bed River." *Germorphology* 114: 326–337.

Mccartney, M., C. Sullivan, and M. Acreman. 2001. "Ecosystem Impacts of Large Dams. School of Arts and Social Sciences Papers".

Merten, G. H., P. D. Capel, and J. P. Minella. 2014. "Effects of Suspended Sediment Concentration and Grain Size on Three Optical Turbidity Sensors." *Journal of Soils and Sediments* 14: 1235–1241. https://doi.org/10.1007/s11368-013-0813-0.

Minella, J. P., G. H. Merten, J. M. Reichert, and R. T. Clarke. 2008. "Estimating Suspended Sediment Concentrations From Turbidity Measurements and the Calibration Problem." *Hydrological Processes* 22, no. 12: 1819–1830.

Misset, C., A. Recking, C. Legout, et al. 2019. "The Dynamics of Suspended Sediment in a Typical Alpine Alluvial River Reach: Insight From a Seasonal Survey." *Water Resources Research* 55, no. 12: 10918–10934. https://doi.org/10.1029/2019WR025222.

Morris, G. L., and J. Fan. 1998. *Reservoir Sedimentation Handbook*. McGraw-Hill Book Co.

Nelson, R. W., J. R. Dwyer, and W. E. Greenberg. 1987. "Regulated Flushing in a Gravel-Bed River for Channel Habitat Maintenance: A Trinity River Fisheries Case Study." *Environmental Management* 11: 479–493.

Némery, J., V. Mano, A. Coynel, et al. 2013. "Carbon and Suspended Sediment Transport in an Impounded Alpine River (isère, France)." *Hydrological Processes* 27, no. 17: 2498–2508. https://doi.org/10.1002/hyp.9387.

Newcombe, C. P., and J. O. Jensen. 1996. "Channel Suspended Sediment and Fisheries: A Synthesis for Quantitative Assessment of Risk and Impact." *North American Journal of Fisheries Management* 16: 693–727.

Olivier, A., G. Pierrefeu, M. Scotti, and B. Blanquart. 2008. "Incertitudes sur les débits issus des courbes de tarage." *Journées de L'hydraulique* 30: 1–7.

Palanques, A., J. Guillén, P. Puig, and J. O. Grimalt. 2020. "Effects of Flushing Flows on the Transport of Mercury-Polluted Particulate Matter From the Flix Reservoir to the Ebro Estuary." *Journal of Environmental Management* 260, no. 4: 110028. https://doi.org/10.1016/J.JENVMAN.2019.110028 https://www.sciencedirect.com/science/article/pii/S0301479719317463.

Pallarès, A., P. Schmitt, and W. Uhring. 2021. "Comparison of Time Resolved Optical Turbidity Measurements for Water Monitoring to Standard Real-Time Techniques." *Sensors* 21, no. 9: 3136. https://doi.org/10.3390/s21093136.

Peter, D. H., E. Castella, and V. I. Slaveykova. 2014. "Effects of a Reservoir Flushing on Trace Metal Partitioning, Speciation and Benthic Invertebrates in the Floodplain." *Environmental Science: Processes & Impacts* 16: 2692–2702. https://doi.org/10.1039/C4EM00387J.

Petts, G., T. Foulger, D. Gilvear, J. Pratts, and M. Thomas. 1985. "Wave-Movement and Water-Quality Variations During a Controlled Release From Kielder Reservoir, North Tyne River, U.K." *Journal of Hydrology* 80: 371–389. https://doi.org/10.1016/0022-1694(85)90129-5.

Petts, G., and A. Gurnell. 2005. "Dams and Geomorphology: Research Progress and Future Directions." *Geomorphology* 71, no. 10: 27–47. https://doi.org/10.1016/j.geomorph.2004.02.015.

Pisaturo, G. R., S. Folegot, A. Menapace, and M. Righetti. 2021. "Modelling Fish Habitat Influenced by Sediment Flushing Operations From an Alpine Reservoir." *Ecological Engineering* 173: 106439. https://doi.org/10.1016/J.ECOLENG.2021.106439.

Provincia Autonoma di Trento. 2006. "Piano generale di utilizzazione delle acque pubbliche." http://www.pguap.provincia.tn.it/.

Rainato, R., L. Martini, G. Pellegrini, and L. Picco. 2021. "Hydrological, Geomorphic and Sedimentological Responses of an Alpine Basin to a Severe Weather Event (Vaia Storm)." *Catena* 207: 105600. https://doi.org/10.1016/j.catena.2021.105600.

Rathburn, S. L., and E. E. Wohl. 2001. "One-Dimensional Sediment Transport Modeling of Pool Recovery Along a Mountain Channel After a Reservoir Sediment Release." *Regulated Rivers: Research & Management* 17, no. 5: 251–273. https://doi.org/10.1002/rrr.617.

Schleiss, A. J., M. J. Franca, C. Juez, and G. D. Cesare. 2016. "Reservoir sedimentation." *Journal of Hydraulic Research* 54, no. 6: 595–614. https://doi.org/10.1080/00221686.2016.1225320.

Stradiotti, G., M. Righetti, T. H. Tarekegn, G. Wharton, and M. Toffolon. 2020. "New Conceptual Framework for the Erosion of Fine Sediment From a Gravel Matrix Based on Experimental Analysis." *Journal of Hydraulic Engineering* 146, no. 9: 04020061. https://doi.org/10.1061/(ASCE)HY.1943-7900.0001795.

Sumi, T., M. Okano, and Y. Takata. 2004. "Reservoir Sedimentation Management With Bypass Tunnels in Japan." In *Proc. 9th International Symposium on River Sedimentation*, 1036–1043. Tsinghua University Press.

Surian, N., L. Mao, M. Giacomin, and L. Ziliani. 2009. "Morphological Effects of Different Channel-Forming Discharges in a Gravel-Bed River." *Earth Surface Processes and Landforms* 1107: 1093–1107. https://doi.org/10.1002/esp.

Tarekegn, T. H., M. Toffolon, M. Righetti, et al. 2014. "Modelling Suspended Sediment Wave Dynamics of Reservoir Flushing." In *Proceedings of the Reservoir Sedimentation—Special Session on Reservoir Sedimentation of the 7th International Conference on Fluvial Hydraulics, River Flow*, 163–173. CRC Press/Balkema.

Tavelli, M., S. Piccolroaz, G. Stradiotti, G. R. Pisaturo, and M. Righetti. 2020. "A New Mass-Conservative, Two-Dimensional, Semi-Implicit Numerical Scheme for the Solution of the Navier-Stokes Equations in Gravel Bed Rivers With Erodible Fine Sediments." *Watermark* 12, no. 3: 1–19. https://doi.org/10.3390/w12030690.

Tena, A., R. Batalla, and D. Vericat. 2012. "Reach-Scale Suspended Sediment Balance Downstream From Dams in a Large Mediterranean River." *Hydrological Sciences Journal* 57, no. 5: 831–849.

Tena, A., D. Vericat, and R. J. Batalla. 2014. "Suspended Sediment Dynamics During Flushing Flows in a Large Impounded River (The Lower River Ebro)." *Journal of Soils and Sediments* 14: 2057–2069. https://doi.org/10.1007/s11368-014-0987-0.

Turowski, J. M., D. Rickenmann, and S. J. Dadson. 2010. "The Partitioning of the Total Sediment Load of a River Into Suspended Load and Bedload: A Review of Empirical Data." *Sedimentology* 57, no. 4: 1126–1146.

van Maren, D. S., M. Yang, and Z. B. Wang. 2011. "Predicting the Morphodynamic Response of Silt-Laden Rivers to Water and Sediment Release From Reservoirs: Lower Yellow River, China." *Journal of Hydraulic Engineering* 137, no. 1: 90–99. https://doi.org/10.1061/(ASCE)HY.1943-7900.0000285.

Van Rijn, L. C. 1984a. "Sediment Transport, Part I: Bed Load Transport." *Journal of Hydraulic Engineering* 110, no. 10: 1431–1456.

Vaughan, M. C. H., W. B. Bowden, J. B. Shanley, et al. 2017. "High-Frequency Dissolved Organic Carbon and Nitrate Measurements Reveal Differences in Storm Hysteresis and Loading in Relation to Land Cover and Seasonality." *Water Resources Research* 53, no. 7: 5345–5363. https://doi.org/10.1002/2017WR020491.

Vercruysse, K., R. C. Grabowski, and R. J. Rickson. 2017. "Suspended Sediment Transport Dynamics in Rivers: Multi-Scale Drivers of Temporal Variation." *Earth-Science Reviews* 166: 38–52.

Vericat, D., and R. J. Batalla. 2006. "Sediment Transport in a Large Impounded River: The Lower Ebro, Ne Iberian Peninsula." *Geomorphology* 79: 72–92. https://www.sciencedirect.com/science/article/pii/S0169555X06000705. https://doi.org/10.1016/J.GEOMORPH.2005.09.017.

Vörösmarty, C. J., M. Meybeck, B. Fekete, K. Sharma, P. Green, and J. P. Syvitski. 2003. "Anthropogenic Sediment Retention: Major Global Impact From Registered River Impoundments." *Global and Planetary Change* 39, no. 1: 169–190 (The supply of flux of sediment along hydrological pathways: Anthropogenic influences at the global scale). https://doi.org/10.1016/S0921-8181(03)00023-7 https://www.sciencedirect.com/science/article/pii/S0921818103000237.

Wang, Z.-Y., and H. Chunhong. 2009. "Strategies for Managing Reservoir Sedimentation." *International Journal of Sediment Research* 24, no. 4: 369–384.

Wharton, G., S. H. Mohajeri, and M. Righetti. 2017. "The Pernicious Problem of Streambed Colmation: A Multi-Disciplinary Reflection on the Mechanisms, Causes, Impacts, and Management Challenges." *Wiley Interdisciplinary Reviews: Water* 4: e1231. https://doi.org/10.1002/wat2.1231.

White, R. 2001. *Evacuation of Sediments From Reservoirs*. Thomas Telford Publishing. https://doi.org/10.1680/eosfr.29538.

Williams, G. P. 1989. "Sediment Concentration Versus Water Discharge During Single Hydrologic Events in Rivers." *Journal of Hydrology* 111: 89–106. https://doi.org/10.1016/0022-1694(89)90254-0.

Wohl, E., B. P. Bledsoe, R. B. Jacobson, et al. 2015. "The Natural Sediment Regime in Rivers: Broadening the Foundation for Ecosystem Management." *Bioscience* 65, no. 3: 358–371. https://doi.org/10.1093/biosci/biv002.

Wohl, E., and A. Cenderelli. 2000. "Sediment Deposition and Transport Patterns Following a Reservoir Sediment Release." *Water Resources Research* 36: 319–333.

Wymore, A. S., M. C. Leon, J. B. Shanley, and W. H. McDowell. 2019. "Hysteretic Response of Solutes and Turbidity at the Event Scale Across Forested Tropical Montane Watersheds." *Frontiers in Earth Science* 7, no. 5: 126. https://doi.org/10.3389/feart.2019.00126.

Zuecco, G., D. Penna, M. Borga, and H. J. van Meerveld. 2016. "A Versatile Index to Characterize Hysteresis Between Hydrological Variables at the Runoff Event Timescale." *Hydrological Processes* 30, no. 9: 1449–1466.

Supporting Information

Additional supporting information can be found online in the Supporting Information section.